ORNL/SPR-2024/3329

NEAMS Burnup Extension Accomplishments and Remaining Modeling Gaps

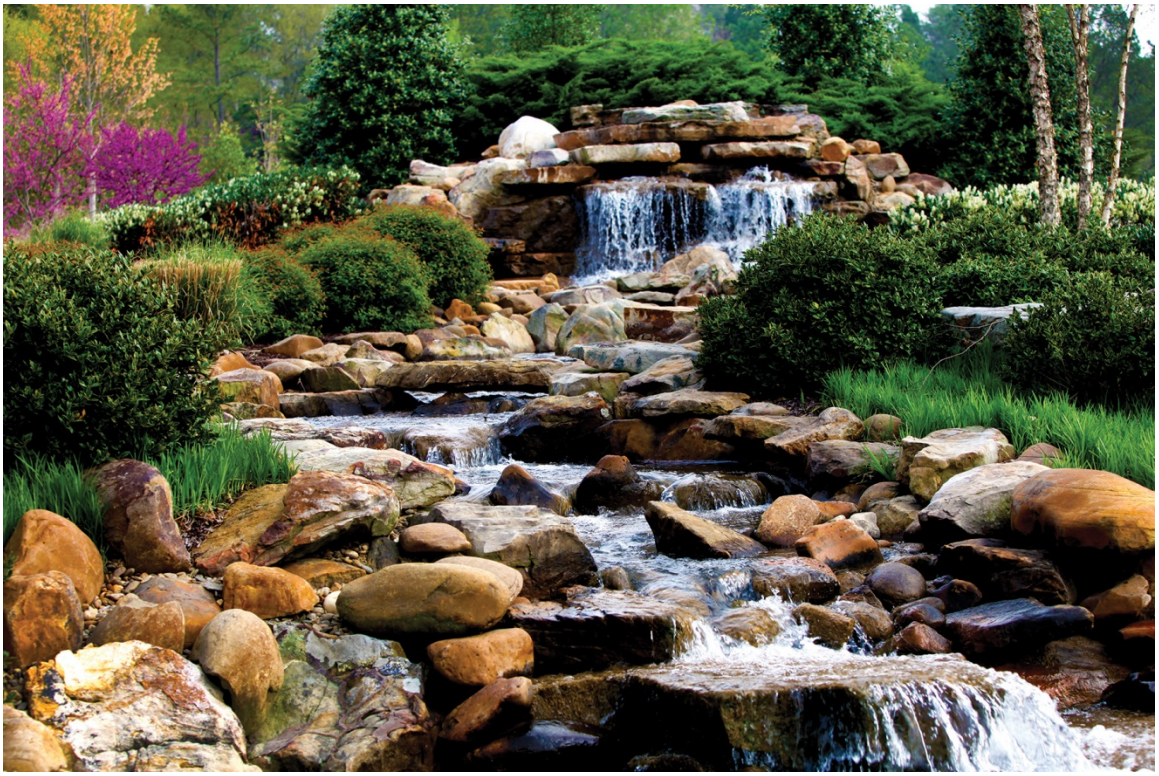

Oak Ridge National Laboratory
Nathan Capps
Ian Greenquist
Danny Schappel
Aaron Wysocki
Robert Salko Jr.

Los Alamos National Laboratory
David Andersson
Conor Galvin
Laurent Capolungo
Andrea Rovinelli
Michael Cooper

Idaho National Laboratory
Stephen Novascone
Ryan Sweet
Pierre-Clément Simon
Larry Aagesen
Sudipta Biswas

Pennsylvania State University
Elia Merzari

Electric Power Research Institute
Brenden Mervin

April 2024

ORNL/SPR-2024/3329

Nuclear Energy Advanced Modeling and Simulation Program

NEAMS BURNUP EXTENSION ACCOMPLISHMENTS AND REMAINING MODELING GAPS

Oak Ridge National Laboratory
Nathan Capps
Ian Greenquist
Danny Schappel
Aaron Wysocki
Robert Salko Jr.

Los Alamos National Laboratory
David Andersson
Conor Galvin
Laurent Capolungo
Andrea Rovinelli
Michael Cooper

Idaho National Laboratory
Stephen Novascone
Ryan Sweet
Pierre-Clément Simon
Larry Aagesen
Sudipta Biswas

Pennsylvania State University
Elia Merzari

Electric Power Research Institute
Brenden Mervin

April 2024

Prepared by
OAK RIDGE NATIONAL LABORATORY
Oak Ridge, TN 37831
managed by
UT-BATTELLE LLC
for the
US DEPARTMENT OF ENERGY
under contract DE-AC05-00OR22725

CONTENTS

LIST OF FIGURES

LIST OF TABLES

ABBREVIATIONS

AOO	anticipated operational occurrence
AFC	Advanced Fuels Campaign
ANS	American Nuclear Society
ATF	accident-tolerant fuel
BDBA	beyond-design-basis accident
BEMUSE	Best Estimate Methods, Uncertainty and Sensitivity Evaluation
CILC	crud-induced localized corrosion
CIPS	crud-induced power shift
CPR	critical power ratio
DBA	design-basis accident
DNB	departure from nucleate boiling
DOE	US Department of Energy
EPRI	Electric Power Research Institute
FFRD	fuel fragmentation, relocation, and dispersal
FFT	fast-Fourier transform
FGP	fission gas produced
FGR	fission gas release
HBS	high-burnup structure
IRA	Inflation Reduction Act
LHR	linear heat rate
LAPX	Los Alamos Polycrystals
LOCA	loss-of-coolant accident
LTA	lead test assembly
LTR	lead test rod
LWR	light-water reactor
M&S	modeling and simulation
MD	molecular dynamics
NEAMS	Nuclear Energy Advanced Modeling and Simulation
NFIR	Nuclear Fuel Industry Research
NRC	US Nuclear Regulatory Commission
O&M	operation and maintenance
OECD	Organisation for Economic Co-operation and Development
PCT	peak clad temperature
PWR	pressurized water reactor
R&D	research and development
RBHT	rod bundle heat transfer
RELAP	Reactor Excursion and Leak Analysis Program
RIL	research information letter
SCIP	Studsvik Cladding Integrity Project
Sifgrs	simplified integrated fission gas release and swelling [model]
SRC	strain rate criterion
tFGR	transient fission gas release
TRACE	TRAC/RELAP Advanced Computational Engine

ABSTRACT

The economic viability of light-water reactors (LWRs) in the United States is declining in heavily subsidized markets, and as a result, the nuclear industry is looking for opportunities to enhance the economic competitiveness of nuclear power. This is not a foreign concept to the nuclear industry: in the mid-2000s, the nuclear industry set out to achieve zero fuel failures by 2010. The goal in this effort was to drive down the cost of reactor shut down by replacing a pin or bundle in response to fuel rod failure. 2010 brought about the initiative to deliver the nuclear promise to reduce operating cost by 30% to improve nuclear energy's economic competitiveness before 2020. The emergence of accident-tolerant fuel also offers the nuclear industry an opportunity to build on these past successes and deliver affordable, clean energy. Accident-tolerant fuel has been shown to provide superior performance compared to traditional Zircaloy/UO_2 fuel concepts, offering the unique ability to remove operational limitations that inhibit the economic viability of nuclear power. This has led the industry to begin building a technical case to extend the peak rod average burnup beyond 62 GWd/tU to extend pressurized water reactor cycle lengths to 24 months and to develop more efficient boiling water reactor core designs.

The Nuclear Energy Advanced Modeling and Simulation (NEAMS) program mission is to develop advanced modeling and simulation tools and capabilities to accelerate the deployment of advanced nuclear energy technologies. The primary safety concern inhibiting the nuclear industry from extending burnup is related to high-burnup fuel fragmentation, relocation, and dispersal. Therefore, the NEAMS program developed a targeted 5-year plan to support the industry's efforts to extend burnup. This milestone report summarizes the 5-year plan that was enacted in FY20, followed by a discussion of the ongoing activates required to fulfill the 5-year plan, as well as the approach to address the current modeling gaps. Additionally, an LWR stakeholder meeting was held to communicate work performed in the NEAMS program over the past three years, to assess the LWR community's perspective on the impact of the program, and to identify remaining significant gaps in the NEAMS suite of capabilities. This engagement will be documented by the Electric Power Research Institute and used by NEAMS to redirect current LWR scope as needed and to develop the next phase for LWR research and development.

1. INTRODUCTION

Nuclear fuel performance and its impact on safety became a topic of emphasis following the March 2011 disaster at the Fukushima Daiichi Nuclear Power Plant. In response to the accident, the US Senate directed the US Department of Energy (DOE) to start developing next-generation light-water reactor (LWR) nuclear fuels with enhanced accident tolerance [1]. Success in this endeavor was defined by the development of a commercialized product that could be broadly used in the existing LWR fleet. The plan, shown in Figure 1, was organized into three phases: (1) feasibility, (2) development/qualification, and (3) commercialization. The feasibility phase prioritized small-scale testing to assess the ability of the concepts to survive under LWR conditions and to identify obstacles. Accident-tolerant fuels (ATFs) where then down-selected and transitioned to the development and qualification phase, where research and development (R&D) activities were implemented to support deployment of lead test rods (LTRs). Completion of phase two was scheduled for 2020 so that ATF concepts could transition from the R&D phase to commercial irradiations (i.e., LTRs and lead test assemblies [LTAs]). However, DOE exceeded all expectations and successfully deployed the first LTR in 2018, and since then, DOE has deployed multiple LTRs and an LTA.

Because of the success of the ATF program, the US nuclear fleet began developing a business case for ATF deployment. The original ATF metrics were designed to facilitate widespread adoption of ATF concepts were as follows:

- Acceptable neutron absorption cross sections
- Amenability to fabrication
- Sufficient supply of raw materials
- Compatibility with current LWR operational conditions
- Ability to meet existing fuel reliability expectations

Although these metrics are valid, they were not sufficient to support industry adoption of ATF and to move away from a safe nuclear fuel. Therefore, the deployment of ATF concepts by the US nuclear fleet became predicated on harvesting margins from the safety benefits afforded by ATF to offset projected implementation costs. This realization led to the Electric Power Research Institute (EPRI) Accident-Tolerant Fuel Valuation study [2], a thorough analysis of ATF safety benefits describing how ATF safety benefits may impact beyond-design-basis accidents (BDBAs), design basis accidents (DBAs), and anticipated operational occurrences (AOOs). The results of the study revealed several safety benefits associated with ATFs, including enhanced mechanical stability under high-temperature conditions and reduced hydrogen production in comparison to Zr/UO_2. A summary of the analysis can be found in Table 6-1 of the EPRI report [2]. The industry's response to the ATF safety benefits suggest that the use of ATF may facilitate the following economic benefits:

- Burnup extension: increase peak rod average burnup beyond 62 GWd/tU and increase pressurized water reactor (PWR) cycle lengths to 24 months

- Departure from nucleate boiling (DNB) and critical power ratio (CPR) margin: change current AOO failure criteria to a cladding-based criteria (i.e., time at temperature)

- Crud / crud-induced power shift (CIPS) reduction: enhanced water chemistry to reduce crud deposition

At the time of these findings, the US nuclear fleet was under tremendous pressure to increase the economic viability of nuclear power. At this writing, the drive to significantly reduce carbon emissions to

meet domestic goals is further driving the need for nuclear power. Costs to operate a nuclear power plant are generally associated with plant operation and maintenance (O&M). Operating costs are associated with the fuel itself resulting from the cost of the materials used to produce the fuel or the cost of the reactor core design. Fuel material costs are generally beyond the utility's control; however, core design optimizations and cycle lengths are within the utility's control, offering the opportunity for significant O&M savings. Core designs are generally constrained by enrichment limits of 5% ^{235}U and a peak rod average burnup limit of 62 GWd/MTU. These limitations also impact the PWR's ability to extend cycle length. Additionally, extending cycle length reduces outages (zero power operation) and maintenance costs making the choice to increase burnup and cycle lengths all the more advantageous. However, to extend burnup, the industry must address all safety concerns, and chief among these concerns is fuel fragmentation, relocation, and dispersal (FFRD).

FFRD was first observed in the Halden loss-of-coolant accident (LOCA) high-burnup (>90 GWd/MTU) integral tests. The issue gained attention when FFRD was also observed closer to the current US operating limit (62 GWd/MTU rod average) at Studsvik Nuclear in early 2011 [3]. This finding triggered the US Nuclear Regulatory Commission (NRC) investigation to assess the possibility of this phenomenon occurring in a LOCA and if the phenomenon and subsequent consequences should be considered in LOCA safety methodologies [3]. The conclusion was that the dispersal of fuel into the reactor coolant system introduces additional complications in LWR fuel safety evaluations. Although existing methodologies were deemed to be adequate for current operation, if burnup could be extended, then FFRD would need to be addressed as a safety concern. Therefore, the US nuclear industry has renewed efforts to build a technical basis to extend the rod-average burnup limit in order to reduce core design constraints, thereby increasing core energy utilization efficiencies. A key component of the technical basis is to successfully disposition FFRD.

A critical review of FFRD was performed outlining a number of conditions [4] contributing to fuel performance during a LOCA. The identified conditions are reported to work in concert to determine the fuel's susceptibly to FFRD, as shown in Figure 1. The first component is the LOCA transient, which triggers a rapid increase in cladding temperature and off-normal temperature gradients across the fuel pellet. This behavior is driven by the abrupt change from a nucleate boiling or boiling condition to a near adiabatic thermal hydraulic condition. Historically, system-level codes such as the Reactor Excursion and Leak Analysis Program (RELAP) or the TRAC/RELAP Advanced Computational Engine (TRACE) have been used to capture the thermal hydraulic evolution of the hot rod. However, because FFRD is a pin-specific phenomenon that differs from the hot rod assumptions, more detailed subchannel thermal hydraulics are required to capture cladding temperature evolution. Furthermore, the abrupt change in cladding temperatures results in cladding deformation, eventual ballooning, and likely rupture during the LOCA transient [4]. This is a critical component to FFRD, because without rupture, fuel will not be dispersed, and without ballooning, relocation is unlikely to occur. Therefore, it is critical to capture the ballooning behavior in the axial and hoop direction, as well as cladding rupture, to determine FFRD susceptibility and severity [5]. Likewise, the rapid profile and magnitude changes in fuel pellet temperature have been shown to release stored fission gas from the pellet which may impact the cladding's ballooning and burst behavior. Conversely, hydrostatic constraints have been shown to reduce the amount of fission gas release (FGR) and fragmentation that may occur during a LOCA event [6]. This highlights the inherent coupled nature between the fuel and cladding performance, which leads directly to the second component: material performance.

Material performance captures the material property's evolution, ultimately putting the fuel in a position to be susceptible to FFRD. It is simple enough to say all current material models used to evaluate Zr/UO_2 are required to evaluate FFRD, but there are more mechanistic material performance considerations beyond the standard models that contribute to FFRD susceptibility:

- Stored energy in the fission gas bubbles (i.e., pressure)
- Degraded fuel material properties
- Mechanical (irradiation or chemical) changes
- Strain energy in the fuel matrix from fission products
- Increase in local stress concentrations (irradiation and/or fission product defects)
- Cladding ballooning, burst timing, and rupture opening
- Steady-state and transient FGR (tFGR) and rod internal pressure

The as-fabricated microstructure—porosity and grain size—is homogeneous throughout the pellet, but it changes substantially during the fission process. As a result of the fuel pellet having nonuniform radial distributions of fission rate, temperature, and stresses, distinctive "white" and "dark" zones are observed in the fuel pellet's microstructure during irradiation. Visibly, the major differences between the two zones are distribution of the fission gas bubbles, the size of the bubbles, and the precipitation of intermetallic defects. The nucleation and growth processes of fission gas bubbles are quite complex. Fission gas bubbles nucleate and form intergranular or intragranular bubbles, and over time, these bubbles diffuse together to form larger bubbles. The amount of gas available to form a bubble and the bubble size distribution, which is primarily radial, depend on the accumulated burnup and the time-dependent radial temperature distribution. Fuel performance characteristics not captured by conventual fuel performance models are associated with the evolution of the fuel pellet's microstructure. Much of the gaps in conventual fuel performance models are associated with the evolution of the fuel pellet microstructure, but cladding performance impacts fuel performance and is specifically associated with the balloon-burst behavior of the cladding. Cladding behavior has been generally accounted for, but the models currently developed were not intended to assess FFRD susceptibility. For example, rupture timing is a critical component, but balloon formation in the axial and hoop directions is an essential factor when evaluating relocation. These models were developed using legacy data to assess flow blockage, but they fail to adequately capture the intermediate temperature regimes (400–700˚C) or the plastic deformation that occurs prior to rupture. This behavior was noted in NRC Research Information Letter (RIL) 2021-13 [5] and extended the discussion to include the impact of the rupture opening.

Lastly, the fuel rod's operational history impacts the preconditioned state of the pellet (microstructure evolution) and the pretransient rod conditions (FGR and rod internal pressure) prior to the transient. This in effect defines the fuel's initial vulnerability to FFRD. The RIL highlights burnup as the primary parameter driving FFRD. However, data generated through the Nuclear Fuel Industry Research (NFIR) [6] program and recent high-burnup microscopy data [7–9] suggest that FFRD may be influenced by the fuel rod's power history (i.e., temperature) and therefore suggests that there may be burnup and fuel temperature thresholds operating in tandem. In parallel, the microstructure evolution directly contributes to the amount of FGR during steady-state operation and in turn increases the rod's internal pressure, which is the force driving cladding deformation during the transient: a higher pressure increases the probability of cladding failure.

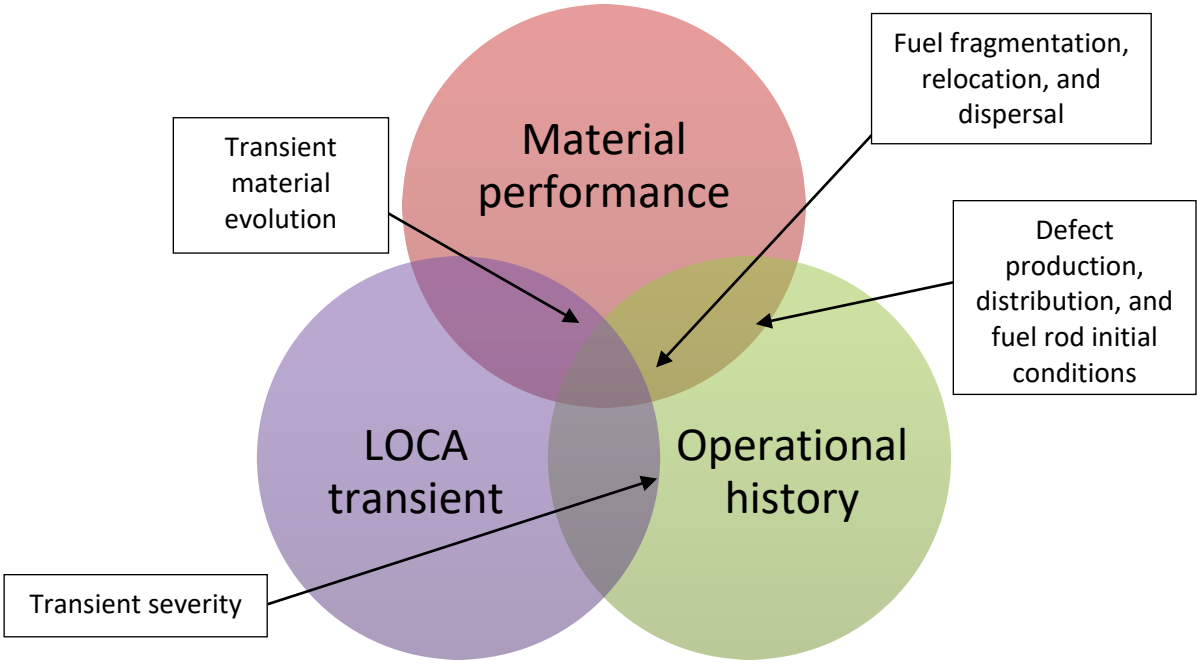

Figure 1. Schematic illustrating the three conditions determining fuel susceptibly to FFRD.

2. MODELING AND SIMULATION PLAN TO SUPPORT BURNUP EXTENSION

Operating conjointly with separate effects testing under the Advanced Fuels Campaign (AFC), the NEAMS program leverages high-fidelity modeling and simulation (M&S) tools to improve understanding of material property evolution and of the pretransient and transient conditions impacting fuel susceptibility to FFRD. Advanced modeling techniques are used to support development of mechanistic models to fill existing technical gaps and to reduce modeling and experimental uncertainties. Results from these efforts inform the LWR industry's high-burnup LOCA safety analysis methodologies. Table 1 summarizes the high-level modeling tasks associated with NEAMS efforts to support high-burnup LOCA modeling.

Table 1. NEAMS 5-year high-level plan to support high-burnup LOCA modeling

Task	Description	Gaps
Full-core LOCA demonstration	Use multiphysics tools to demonstrate code capabilities to assess high-burnup steady-state and LOCA conditions and to assess FFRD susceptibility	• Code coupling status and workflow procedure • Transient capabilities • Code limitations and model gaps • Demonstration assumptions
Mechanistic material model development	• Address immediate material model gaps through development and implementation of empirical models • Develop and implement mechanistic material models informed by lower length scale physics	• Transient FGR fragmentation/ pulverization • Cladding viscoplastic performance • Rupture opening geometry
Lower length scale	• Apply lower length scale modeling techniques to understand the mechanisms contributing to high-burnup fuel performance • Analyze results to inform development of mechanistic material models	• FG bubble pressure evolution • FG bubble over-pressurization and UO_2 fracture • Grain restructuring
Model validation	Compare mechanistic models to publicly available data and benchmark to existing models	• Validation of BISON to high burnup fuel performance • Quantification of material model uncertainty

Multiphysics tools have been used from the onset of these efforts to perform a full-core LOCA demonstration in support of industry's objective to extend burnup. This demonstration required heavy industry engagement and the use of NEAMS tools to simulate a core containing high-burnup fuel with a full-core LOCA. A key objective of the analysis was to identify the limiting LOCA condition, which in turn required a detailed analysis of the conditions driving FFRD susceptibility, such as fuel rod / assembly burnup, peak clad temperature (PCT), cladding rupture, and so on. The goal of this approach is to leverage VERA-CS to perform equilibrium core depletion analyses (power history, axial profile, thermal boundary condition, flux, and so on) for every rod in the core, as well as appropriate LOCA decay heat profiles [10]. NEAMS does not have a transient thermal hydraulic tool, so NRC TRACE will be used to develop the LOCA thermal hydraulic boundary conditions [11]. VERA-CS and TRACE results will be passed to BISON for the transient fuel performance and FFRD susceptibility evaluation [12].

In parallel, lower length scale modeling techniques will be used to support development of mechanistic models to fill current knowledge gaps, to reduce modeling and experimental uncertainties, and to ultimately inform the aforementioned full-core LOCA demonstration and industry's high-burnup LOCA safety analysis methodologies. The approach relies on application of M&S tools to gain an understanding of the phenomenon responsible for increasing the fuel susceptible to FFRD and can be used to physically inform existing models. These physically informed models can then be deployed in engineering scale codes such as BISON to isolate the conditions that lead to and/or preclude FFRD by effectively designing to create the operating conditions under which FFRD is less likely to occur. These models will require continuous refinement and validation as large-scale integral LOCA data, separate effects data, and high-fidelity microscopy data become available. Figure 2 provides an illustration of the NEAMS workflow for burnup extension, and a detailed summary of the accomplishments to date can be found in Appendix A.

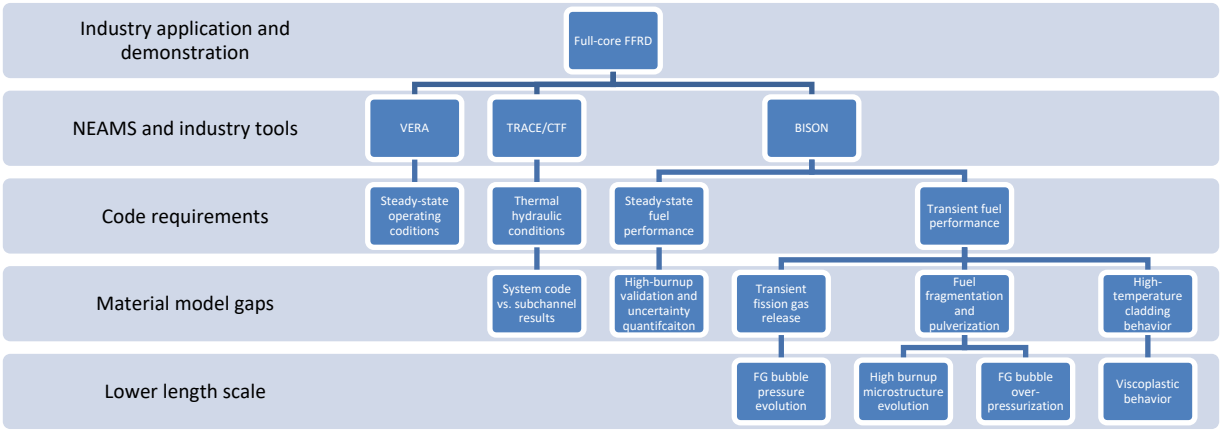

Figure 2. Schematic illustrating the NEAMS workflow to support high-burnup LOCA modeling.

3. LIGHT-WATER REACTOR STAKEHOLDER FEEDBACK

Stakeholders from the industry assembled on March 14–15, 2024 at the EPRI offices in Charlotte, North Carolina, along with NEAMS staff, to receive a briefing on the status of NEAMS burnup extension activities. The industry participants and their organizations are listed in Table 2. The goal of this meeting was to review and summarize the status of NEAMS burnup extension five-year plan and to identify high impact M&S research and code capability gaps for the LWR community. Additionally, feedback from the LWR stakeholders will be used to guide the subsequent NEAMS LWR five-year plan. NEAMS staff spent one day briefing the industry on modeling status and accomplishments, and a half day was spent aggregating industry feedback and delivering that feedback to NEAMS and DOE. This section summarizes the identified gaps and actionable feedback to inform the development of the subsequent five-year plan.

Table 2. List of industry participants at the LWR stakeholder meeting

Organization	Name
Duke Energy	Stanley Hayes, Duncan Robinson
D Schrire Nuclear Fuel Performance AB	David Schrire
EPRI	Mohammed Abdoelatef, Brenden Mervin, Kurshad Muftuoglu, Suresh Yagnik, Ken Yueh
Framatome, Inc.	Lisa Gerken
NRC	Andrew Bielen, James Corson*
Global Nuclear Fuel	Ian Porter*
Structural Integrity Associates Inc.	Joe Rashid
Veracity Nuclear LLC	David Kropaczek
Westinghouse Electric Company LLC	Kevin Barber, Jeffrey Kobelak, Yun Long

*Follow-up one-on-one meetings

The modeling areas are ranked based on the value opportunities available within each area in Table 3. Areas with higher rankings were identified to have more phenomenological uncertainty, more opportunities for improved fundamental understanding of the underlying mechanisms, and/or more industry impact if additional understanding or modeling capacity is gained. It was also stated that most of the topics shown in Table 3 are inherently coupled and likely should be addressed in parallel or at least with knowledge of the impact that the other topics may have on the phenomenon.

Table 3. Ranking of important modeling areas supporting burnup extension within NEAMS

Rank	Modeling area	Planned Scope	Stakeholder Feedback	Additional Requirements
1	Axial gas communication	Initial model development and capability implementation	Current industry tools are not equipped to model this phenomenon	**Coupled to Item 7** - Development and application of model for to support validation to separate effects and integral test for PWR and BWR conditions
2	Fuel-clad bonding and HBS	**Coupled to Item 1** - Initial model development and couple to axial gas communication	Current industry tools are not equipped to model this phenomenon	**Coupled to Item 1 and 7** Development and application of model for pellet-cladding contact and bonding
3	Nondiffusional FGR	**Coupled to item 4 and 6 -** Complete development of a mechanistic high burnup tFGR model Implement an empirical tFGR model	No relevant model available	Complete model development and refine models to better understand observed phenomenon
4	Fuel fragmentation and pulverization	**Coupled to item 3** - Complete development of a mechanistic high burnup fuel restructuring model capable of addressing both the rim and mid-region of the fuel pellet **Coupled to item 3** - Characterization of fracture and micro-cracking at grain boundary bubbles in UO_2 by MD simulations	Source of high uncertainty and no model capable of estimating particle size.	Validation of first-generation advanced FFRD models against separate effects and integral test for PWR and BWR conditions
5	Thermal hydraulics	Complete CTF validation to experimental LOCA data and benchmark to system code results for high burnup core	Incorporate dispersed mass transport	Major code development
6	Diffusional FGR	**Coupled to item 3** - Complete development and Bison implementation of a model for pressure evolution of fission gas bubbles on UO_2 grain boundaries	Develop a deeper understanding on specific microstructural aspects of fission gas release	Complete development and demonstration of first-generation mechanistic model
7	High-temperature cladding deformation	Complete surrogate model development for Zircaloy	Reduce uncertainties associated with peak balloon strain, axial balloon deformation, and rupture timing	Validation of advanced model Zircaloy ROM models against separate effects and integral test for PWR and BWR conditions **Coupled to Item 1 and 2** - Cladding rupture analysis based on advanced constitutive Zircaloy ROM model

Axial gas communication is the number one priority because of how difficult it is to model and the lack of model availability within the industry. This phenomenon is also coupled with fuel-clad bonding, FGR,

and fuel fragmentation and pulverization, highlighting the reasons these topics are higher on the prioritization list. It is also important to note that nondiffusional FGR is of particular importance to BWRs because the objective for these reactors is to prevent cladding rupture to mitigate FFRD concerns during a LOCA. Thus, the top three modeling areas in Table 3 are all considered to be of near equal importance, and although fuel fragmentation and pulverization are combined as a single phenomenon, it is not as important to BWRs.

In the area of axial gas communication, the ability to predict existing measurements is one of the desired end states; such a model could have value when integrated into specific industry applications.

In the area of fuel-clad bonding, the ability to predict when and where a pellet will break when bonded, the ability to predict when the HBS disintegrates, and the ability to predict thicknesses of the HBS were all identified as useful desired end states.

In the area of nondiffusional FGR, it was found that some existing models did not appear to be consistent with available experimental data (e.g., models correlating FGR to surface area of the particles). The recommendation here is to consider the available experimental data and work on refining models in this area. It was acknowledged that FGR is one of the most difficult areas to model because of the sparse experimental data set and significant knowledge gaps in terms of understanding its major driving forces. Thus, a desired end state is not necessarily to resolve FGR for all cases, but to be able to gain a more compartmentalized understanding on specific aspects of FGR, and perhaps models, methods, and/or recommendations for modeling FGR for different transients is a more obtainable goal. The industry would benefit significantly if a comprehensive model consisting of steady state diffusional FGR, non-diffusional FGR, and gaseous swelling in the fuel during transients were developed and validated. Gaps in industry knowledge associated with the coupled affect between the three phenomena are sources of high uncertainty and importance for mitigating fuel rod failures. It is critical that this model be able to capture the effects of large grain UO_2 and doped UO_2. These characteristics are especially important because fuel dopants are being implemented across the industry, and most dopants have significant impacts on FGR characteristics (both steady-state and during transients) compared to undoped UO_2.

Historically, FGR models primarily capture xenon diffusion and subsequent release from fuel into the free volume, and these models do not capture the diffusion and release of non-traditional isotopes such as iodine. This topic is of particular importance with the ongoing discussions surrounding NUREG 1.183rev2, and the industry sees value in developing this capability to support source term evaluations.

The thermal hydraulic area could become increasingly more important, depending on the NRC's rulemaking decision and whether models are required for (1) mass transport of fuel outside the fuel rod following burst or (2) cladding temperature post-burst. Determining particle transport direction following dispersal, analyzing the impact of temperatures assuming the mass accumulates in certain areas, and determining how fuel fragments could be impacted into spacer grids and affect thermal hydraulic conditions, and thus cladding temperatures, currently represents an area of high uncertainty, and most tools do not have the necessary fidelity to explicitly model this.

High-temperature cladding deformation is ranked last because fuel vendors must conduct their own work on this front. However, there was common agreement that understanding axial balloon deformation and peak balloon strain will have value because this is currently outside of historical safety analyses. This topic is of particular importance when considering burnup extension and power uprates where cladding performance under limiting operational occurrences expands well outside the normal conditions being considered.

Another topic not listed in Table 3 is hydrogen pickup and the impact of hydrogen on cladding mechanical performance. This topic is critical to burnup extension and other topics such as power uprates

where hydrogen pickup and embrittlement are expected to become more prevalent the longer the fuel operates in the reactor. It would be important for such a model to capture why accelerated hydrogen pickup occurs and under what conditions (i.e., power level, coolant chemistry, etc.).

One overarching challenge communicated by the industry was for NEAMS to develop the models and the mechanistic understanding of underlying physical phenomena needed to explain at least some if not all (stretch goal) of the scatter in the data shown in Figure 3. Several hypotheses were discussed, including the relevance of the power history on these data, the differences between BWR and PWR fuel, and whether the x-axis for such a plot is the correct independent variable to compare these data. Being able to explain the reason for the scatter from a fundamental physics standpoint can help significantly address conservatisms.

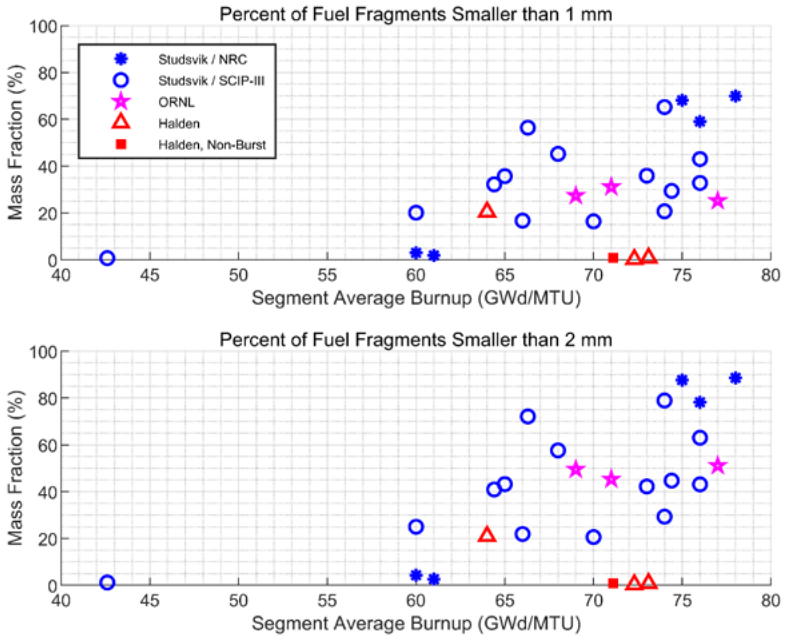

Figure 3. Measurements of percent of fuel fragments smaller than 1 mm and 2 mm as a function of burnup [5].

Another specific challenge is for NEAMS to use their tools to perform blind tests of model predictability before conducting experimental tests. It is recognized that the first few attempts at these blind tests in areas where there is little experimental data will be difficult and may not reproduce reliable experimental results. However, continued efforts and later success will have a significant impact on the confidence and usefulness of these models as tools for industry cross-checks, especially because so many of these areas lack enough validation data to gain modeling confidence in the traditional sense.

Along with the challenge of performing blind tests is the need to quantify modeling uncertainties. When identifying which applications will utilize these models, it is important to understand which models are based on fundamental physics principles, which models are empirical in nature, and which models lie somewhere between those two extremes It is not likely feasible to develop absolute uncertainty estimates for all models, but some bounds must be developed to gauge the confidence of each model in various operating windows and application areas. Additional evaluations using NEAMS tools on impactful industry problems will help the industry understand how these tools are used and how they can be useful. Such demonstrations can also serve as starting points for industry applications. If direct usage of NEAMS tools is envisioned as a goal of the NEAMS program, then developing job aids (not necessarily

methodologies) and disseminating application-specific best practices will also be valuable in the adoption of any NEAMS tools directly by the industry, because use of these tools tends to require significant experience to ensure the correct modeling options are selected for specific applications.

The ability to gain resolution on the mechanistic understanding in many of the areas of interest is also important, and modeling is primed to accomplish this task. Resolution does not necessarily translate to a complete explanation of the phenomenon and an accurate model that covers it. This type of resolution could simply bound the model with uncertainty limits.

The industry also identified several opportunities for engagement.

1. Review available AFC data and identify meaningful validation opportunities and other means of leveraging the data to support NEAMS work. Encourage more cooperation between AFC (experimental) and NEAMS (modeling).

2. Work with industry members who identify other data opportunities available on axial gas communication and other topics from Halden, Studsvik Cladding Integrity Project (SCIP)-III, and others.

3. Examine other opportunities to obtain meaningful high-burnup data from Europe because they operate annual cycles and have a significant inventory of higher burnup fuel.

4. Identify opportunities for industry to provide representative operating conditions, core designs, and so on, for NEAMS analyses to be more generally applicable and impactful.

Aside from burnup extension, other areas that NEAMS should prioritize, include CIPS / crud-induced localized corrosion (CILC) for PWRs, time at temperature for BWRs, and time at temperature for PWRs. It is worth noting that these topics are all coupled with burnup extension. For example, CILC may show increased risk when moving to 24-month cycles, and 24-month cycles are only feasible for high power density plants with burnup extension and increased enrichment. Therefore, as soon as burnup extension becomes allowed, CILC risk mitigation becomes an issue. Because the industry is preparing for burnup extension, cycle length extension, and power uprates, CILC is already being examined.

In summary, industry experts see the potential for NEAMS models and methods to support burnup extension activities, specifically in areas where enhanced fundamental understanding is needed and previous experimental results, experimental opportunities, and data are scarce. However, high confidence is needed in order to look to NEAMS to prove that these tools can be applied in the modeling areas of importance and that tangible value can be extracted and utilized. Presently, modeling assumptions, unknown uncertainties, and lack of validation[1] prevent industry from directly using the methods to support burnup extension. Fortunately, several experimental opportunities support burnup extension–related work, and NEAMS can help define the experimental parameters and validate their methods with these experiments. Significant successes in these areas will provide the confidence needed to enable use of NEAMS models and tools to support license extension activities.

[1] Industry members recognize that they have a role to play in validation because they have access to more of the data required. Therefore, where opportunities exist, industry should collaborate with NEAMS on validation activities. Future work should involve identifying which models have data validation needs, what an acceptable validation state of the model is, and what industry data are available to accomplish the necessary validation.

4. SUMMARY

NEAMS is in the process of demonstrating LWR code capabilities, initial development and implementation code capabilities and mechanistic model requirements to model FFRD, and code validation more specifically up to dispersal susceptibility. This milestone report provides a discussion of the work performed to date and briefly summarizes the initial plans. In general, the NEAMS team has successfully demonstrated the ability for NEAMS tools to evaluate core-wide FFRD (Appendix A.1.1). NEAMS tools will be used to perform a similar evaluation for BWRs. This evaluation highlighted high-temperature cladding performance, tFGR, and fuel fragmentation and pulverization as either a model gap or a source of high uncertainty. The milestone report highlights the efforts of NEAMS over the past three years to address these material mode gaps (Section **Error! Reference source not found.**). These models are under active development, and plans are to have these models successfully implemented into BISON, with initial validation efforts underway. During FY25, the team will continue making improvements to the models and enhancing validation to experimental data to support LWR stakeholder needs. Additional gaps were identified through the process that have also been addressed. TRACE was used for the full-core demonstration, and the LWR stakeholder indicated that a subchannel approach may provide additional value. This required validation of CTF (Section **Error! Reference source not found.**), and eventual benchmarking of CTF to TRACE for high-burnup application (Section **Error! Reference source not found.**). Finally, an empirical rupture opening model was developed and implemented into BISON to support dispersal susceptibility evaluations [31].

An LWR stakeholder meeting was held in March of 2024 to review the progress made toward supporting burnup extension and to identify any remaining gaps (capability or model) not currently being addressed. Two gaps where identified: (1) axial gas communication, and (2) fuel cladding bonding. Axial gas communication is a phenomenon in which the gas (fill gas and released fission gas) within the fuel rod moves from one location to another. It has been shown with experimental data that gas does not instantaneously respond within the rod, and therefore, it impacts local and global rod internal pressures, cladding balloon and burst behavior, tFGR, and fuel fragmentation. Fuel cladding bonding and debonding is a phenomenon that may play a role in cladding balloon and burst. The mechanism in question is to develop the ability to predict (1) the degree to which the bond affects cladding ballooning, and (2) the time at which fuel cladding bonding ultimately fractures during a LOCA. This behavior would initially prevent cladding balloon deformation and may impact the final balloon geometry and rupture timing. It should be noted that these two phenomena are currently being addressed within the program, albeit at a much lower priority level. Although the fuel bonding work is in the preliminary stage, at this stage in FY24, the capability to mitigate clad ballooning and connect porosity to the plenum has been demonstrated. This capability is expected to be merged with the BISON repository later this summer, further expanding the current 2D axial gas communication capability mentioned in Section **Error! Reference source not found.**.

The LWR community is developing a technical basis to support burnup extension, and with the Inflation Reduction Act (IRA) tax credits for nuclear power and generation of clean hydrogen, the technical basis has led to the prioritization of large-scale power uprates in parallel to burnup extension. In addition, LWR stakeholders will be required to address current operating restrictions such as CIPS and CILC. The intent is to build the technical basis to support burnup extension and power uprates by 2027, making nuclear power more economical, and taking advantage of the IRA tax credits by 2030. These considerations will be taken into account and worked into NEAMS future work.

5. REFERENCES

1. S. M. Bragg-Sitton, and J. W. Carmack. "Overview of LWR Accident Tolerant Fuel Development in the United States." *Transactions of the American Nuclear Society*, 2016. https://www.osti.gov/biblio/22992052.
2. EPRI. *Accident-Tolerant Fuel Valuation: Safety and Economic Benefits* (Revision 1), EPRI Technical Report 3002015091, 2019.
3. P. A. C. Raynaud. *Fuel Fragmentation, Relocation, and Dispersal during the Loss-of-Coolant Accident*, NUREG-2121, 2012.
4. N. Capps, C. Jensen, F. Cappia, J. Harp, K. Terrani, N. Woolstenhulme, D. Wachs. "A Critical Review of High Burnup Fuel Fragmentation, Relocation, and Dispersal under Loss-Of-Coolant Accident Conditions," *Journal of Nuclear Materials*, Volume 546, 152750, 2021.
5. NRC. "Interpretation of Research on Fuel Fragmentation, Relocation, and Dispersal at High Burnup." RIL 2021-13, 2021.
6. J. A. Turnbull, S. K. Yagnik, M. Hirai, D. M. Staicu and C. T. Walker. "An Assessment of the Fuel Pulverization Threshold during LOCA-Type Temperature Transients," *Nuclear Science and Engineering*, 179:4, 477–485, DOI: 10.13182/NSE14-20, 2015.
7. J. Noirot, R. Dowek, I. Zacharie-Aubrun, T. Blay, M. Cabié, et al. "Restructuring in High Burn-Up Pressurized Water Reactor UO_2 Fuel Central Parts: Experimental 3D Characterization by Focused Ion Beam—Scanning Electron Microscopy." *Journal of Applied Physics*, 132 (19), p. 195902, 2022.
8. C. McKinney, R. Seibert, J. Werden, C. Parish, T. Gerczak, J. Harp, N. Capps, "Characterization of the Radial Microstructural Evolution in LWR UO_2 Using Electron Backscatter Diffraction," *Journal of Nuclear Materials*, Vol. 585, 154605, ISSN 0022-3115, 2023.
9. T. J. Gerczak, C. M. Parish, P. D. Edmondson, C. A. Baldwin, K. A. Terrani, "Restructuring in High Burnup UO_2 Studied Using Modern Electron Microscopy," *Journal of Nuclear Materials*, Vol. 509, pp. 245–259, 2018.
10. B. Kochunas, B. Collins, S. Stimpson, R. Salko, D. Jabaay, A. Graham, Y. Liu, K. S. Kim, W. Wieselquist, A. Godfrey, K. Clarno, S. Palmtag, T. Downar, J. Gehin, "VERA Core Simulator Methodology for Pressurized Water Reactor Cycle Depletion," *Nuclear Science and Engineering*, 185:1, 217–231, 2017. DOI: 10.13182/NSE16-39.
11. NRC, *TRACE V5.0 Users Guide - Volume 1: Input Specification*. ML120060239, Final. 2008.
12. R. L. Williamson, N. A. Capps, W. Liu, et al. "Multi-Dimensional Simulation of LWR Fuel Behavior in the BISON Fuel Performance Code," JOM 68, 2016.
13. N. Capps et al. "Full Core LOCA Safety Analysis for a PWR Containing High Burnup Fuel." *Nucl. Eng. Des.* 379: 1–22. 2021. doi: 10.1016/j.nucengdes.2021.111194.
14. N. Capps et al. *Full Core LOCA Safety Analysis for a PWR Containing High Burnup Fuel.* ORNL/TM-2020/1700. 2022. Oak Ridge: Oak Ridge National Laboratory.
15. S. Palmtag, A. Godfrey, M. Baird, and E. Walker. *VERAIn User's Manual.* United States: 2022. Web. doi:10.2172/1888918Reference for WBN1 benchmark.
16. A. T. Godfrey, B. S. Collins, C. A. Gentry, S. G. Stimpson, and J. A. Ritchie, *Watts Bar Unit 2 Startup Results with VERA*. 2017. Web. doi:10.2172/1355891.

17. J. A. Turnbull, S. K. Yagnik, M. Hirai, D. M. Staicu and C. T. Walker, "An Assessment of the Fuel Pulverization Threshold during LOCA-Type Temperature Transients," *Nuclear Science and Engineering*, 179:4, 477–485, 2015. DOI: 10.13182/NSE14-20.

18. I. Greenquist, N. Capps, "Effects of Transient Fission Gas Release on Rod Balloon Burst Behavior during a Loss-of-Coolant Accident," *Annals of Nuclear Energy*, Vol. 196, 110213, ISSN 0306-4549, 2024. https://doi.org/10.1016/j.anucene.2023.110213.

19. N. Capps, L. Aagesen, D. Andersson, O. Baldwin, W. C. Brinkley, M. W.D. Cooper, J. Harp, S. Novascone, P.C. A. Simon, C. Matthews, B. D. Wirth, "Empirical and Mechanistic Transient Fission Gas Release Model for High-Burnup LOCA Conditions," *Journal of Nuclear Materials*, Vol. 584, 154557, 2023, https://doi.org/10.1016/j.jnucmat.2023.154557.

20. Y. Pontillon, M. P. Ferroud-Plattet, D. Parrat, S. Ravel, G. Ducros, C. Struzik, I. Zacharie-Aubrun, G. Eminet, J. Lamontagne, J. Noirot, and A. Harrer. "Experimental and Theoretical Investigation of Fission Gas Release from UO_2 up to 70 GWd/t under Simulated LOCA Type Conditions: The GASPARD Program. *Proceedings of the 2004 International Meeting on LWR Fuel Performance*, pp. 490–499, 2004.

21. T. Barani, E. Bruschi, D. Pizzocri, G. Pastore, P. Van Uffelen, R. L. Williamson, L. Luzzi, "Analysis of Transient Fission Gas Behaviour in Oxide Fuel Using BISON and TRANSURANUS," *Journal of Nuclear Materials* Vol. 486, pp. 96–110, 2017. https://doi.org/10.1016/j.jnucmat.2016.10.051.

22. D. Schappel, N. Capps, "Impact of LWR Assembly Structural Features on Cladding Burst Behavior under LOCA Conditions," Nuclear Engineering and Design Vol. 418, 112887, 2024. https://doi.org/10.1016/j.nucengdes.2023.112887.

23. N. Capps, A. Wysocki, A. Godfrey, B. Collins, R. Sweet, N. Brown, S. Lee, N. Szewczyk, and S. Hoxie-Key. "Full Core LOCA Safety Analysis for a PWR Containing High Burnup Fuel." *Nuclear Engineering and Design* Vol. 379, 111194, 2021. doi:https://doi.org/10.1016/j.nucengdes.2021.111194.

24. N. Capps, J. Hirschhorn, A. Wysocki, I. Greenquist, I. *Assessment of the Effect of Prototypic High-Burnup Operating Conditions of Fuel Fragmentation, Relocation, and Dispersal Susceptibility*. Oak Ridge National Laboratory Technical Report, ORNL/SPR-2022/2597, 2022.

25. R. Salko, A. Wysocki, T. Blyth, A. Toptan, J. Hu, V. Kumar, C. Dances, W. Dawn, Y. Sung, V. Kucukboyaci, W. Gurecky, T. Lange, X. Zhao, J. Rader, C. Jernigan, B. Collins, M. Avramova, J. Magedanz, S. Palmtag, K. Clarno, D. Kropaczek, B. Hizoum, A. Godfrey, D. Pointer, J. Turner, R. Sankaran, R. Schmidt, R. Hooper, R. Bartlett, M. Baird, M. Pilch. "CTF: A Modernized, Production-Level, Thermal Hydraulic Solver for the Solution of Industry-Relevant Challenge Problems in Pressurized Water Reactors." *Nuclear Engineering and Design* 397, 111927. 2022. URL: https://www.sciencedirect.com/science/article/pii/S0029549322002783, doi:https://doi.org/10.1016/j.nucengdes.2022.111927.

26. P. Ihle, K. Rust, *FEBA—Flooding Experiments with Blocked Arrays Data Report 1, Test Series I through IV.* Technical Report KfK 3658. Institut fur Reaktorbauelemente Projekt Nukleare Sicherheit. 1984.

27. S. M. Bajorek, F. B. Cheung, "Rod Bundle Heat Transfer Thermal-Hydraulic Program." *Nuclear Technology* 205, 307–327, 2019.

28. R. Salko, A. Wysocki, B. Hizoum, N. Capps, "Assessment of CTF for Modeling of a Large-Break Loss-of-Coolant Accident Reflood Transient," 2024, Manuscript submitted for publication.

29. R. Salko, A. Wysocki, B. Hizoum, N. Capps, "A Study on the Impact of Using a Subchannel Resolution for Modeling of Large Break Loss of Coolant Accidents," 2024, Manuscript submitted for publication.

30. T. Barani et al. "Modeling High Burnup Structure in Oxide Fuels for Application to fuel performance codes. Part I: High Burnup Structure Formation." *Journal of Nuclear Materials*, 539:152296, 2020.

31. N. Capps and R. Sweet. "Model for Determining Rupture Area in Zircaloy Cladding under LOCA Conditions." *Nuclear Engineering and Design*, 401, 112096, 2023.

32. K. A. Gamble, *Axial Relocation Model Extension in BISON*. Idaho National Laboratory, 2018. Web. doi:10.2172/1605203.

33. K. A. Gamble et al. *Advancements in Modeling Fuel Pulverization and Cladding Behavior during a LOCA*. INL/EXT-21-64705-Rev000. Idaho National Laboratory, Idaho Falls, ID, 2021.

34. K. A. Gamble et al. *Evaluation of Mechanistic and Empirical Models against Existing FFRD and LOCA Experimental Databases*. No. INL/ INL/RPT-22-69625. Idaho National Laboratory, Idaho Falls, ID, 2022.

35. C. Genoni et al. "Modeling and Measurement of Axial Gas Transport in Nuclear Fuels." *Transactions of the American Nuclear Society*, 128, 416-419, 2023.

36. L. O. Jernkvist and A. Massih. *Model for Axial Relocation of Fragmented and Pulverized Fuel Pellets in Distending Fuel Rods and Its Effects on Fuel Rod Heat Load*. Technical Report SSM-2015:37, Stråls säkerhets myndigheten, 2015.

37. P. C. A. Simon et al. *Compare Predictions of Transient Fission Gas Release by Empirical and Mechanistic Models to Experiments in High Burnup UO_2 fuel*. Tech. Rep. INL/RPT-23-75026, Idaho National Laboratory, Idaho Falls, ID United States, 2023.

38. R. L. Williamson et al. "BISON: A Flexible Code for Advanced Simulation of the Performance of Multiple Nuclear Fuel Forms." *Nuclear Technology*, *207*(7), pp. 954–980. 2021.

39. T. Wiss et al. "Properties of the High Burnup Structure in Nuclear Light Water Reactor Fuel." *Radiochimica Acta*, 105(11), 893–906, 2017.

40. M. Oguma, "Cracking and Relocation Behaviour of Nuclear Fuel Pellets during Rise To Power," *Nuclear Engineering and Design*, 76, 35–45, 1983.

41. L. O. Jernkvist and A. R. Massih. "Modeling Axial Relocation of Fragmented Fuel Pellets inside Ballooned Cladding Tubes and Its Effects on LWR Fuel Rod Failure Behavior during LOCA." In *Transactions of SMIRT-23*. Manchester, UK, 2015.

42. O. Coindreau, F. Fichot, and J. Fleurot. "Nuclear Fuel Rod Fragmentation under Accidental Conditions." *Nuclear Engineering and Design*, 255:68–76, 2013.

43. L. A. Walton and J. E. Matheson. "FUMAC - A New Model for Light Water Reactor Fuel Relocation and Pellet-Cladding Interaction." *Nuclear Technology*, 64:127–138, 1984.

44. T. Barani, D. Pizzocri, G. Pastore, L. Luzzi, and J.D. Hales. "Isotropic Softening Model for Fuel Cracking in BISON." *Nuclear Engineering and Design*, 342:257–263, 2019. doi:10.1016/j.nucengdes.2018.12.005.

45. J. A. Turnbull et al. "An Assessment of the Fuel Pulverization Threshold during LOCA-Type Temperature Transients." *Nuclear Science and Engineering* 179.4 (2015): 477–485.

46. G. Pastore, L. Luzzi, V. Di Marcello, and P. Van Uffelen. "Physics-Based Modelling of Fission Gas Swelling and Release in UO_2 Applied to Integral Fuel Rod Analysis." *Nuclear Engineering and Design*, 256:75–86, 2013.

47. A. T. Donaldson, T. Healey, and R. A. L. Horwood. *Biaxial Creep Deformation Of Zircaloy-4 PWR Fuel Cladding in the Alpha,(alpha + beta) and Beta Phase Temperature Ranges*. Technical Report, British Nuclear Energy Society, 1985.

48. F. J. Erbacher, H. J. Neitzel, H. Rosinger, H. Schmidt, and K. Wiehr. "Burst Criterion of Zircaloy Fuel Claddings in a Loss-of-Coolant Accident. In *Zirconium in the Nuclear Industry, Fifth Conference*, ASTM STP 754, D.G. Franklin Ed., 271–283. American Society for Testing and Materials, 1982.

49. D. Kaddour, S. Frechinet, A.F. Gourgues, J.C. Brachet, L. Portier, and A. Pineau. "Experimental Determination of Creep Properties of Zirconium Alloys together with Phase Transformation." *Scripta Materialia*, 51(6):515–519, 2004.

50. R. H. Chapman, J. L. Crowley, A. W. Longest, and G. Hofmann. "Zirconium Cladding Deformation in a Steam Environment with Transient Heating." In *Zirconium in the Nuclear Industry*. ASTM International, 1979.

51. V. Di Marcello, A. Schubert, J. van de Laar, and P. Van Uffelen. "The TRANSURANUS Mechanical Model for Large Strain Analysis." *Nuclear Engineering and Design*, 276:19–29, 2014.

52. J. V. Cathcart, R. E. Pawel, R. A. McKee, R. E. Druschel, G. J. Yurek, J. J. Campbell, and S. H. Jury. *Zirconium Metal-Water Oxidation Kinetics, IV. Reaction Rate Studies*. Technical Report ORNL/NUREG-17, Oak Ridge National Laboratory, 1977.

53. S. Leistikow, G. Schanz, H. v. Berg, and A.E. Aly. *Comprehensive Presentation of Extended Zircaloy-4/Steam Oxidation Results 600-1600 C. In CSNI/IAEA Specialists Meeting on Water Reactor Fuel Safety and Fission Product Release in Off-Normal and Accident Conditions*. Riso Nat. Lab., Denmark, 1983.

54. J. T. Prater and E. L. Courtright. *Zircaloy-4 Oxidation at 1300 to 2400 °C.* Technical Report NUREG/CR-4889, PNL-6166, Pacific Northwest Lab, 1987.

55. Light-Water-Reactor Safety Research Program: Quarterly Report, July–September 1976. Argonne National Laboratory, , 1976. Web. doi:10.2172/7116800.

56. B. Kombaiah and K. Linga Murty. "Dislocation Cross-Slip Controlled Creep in Zircaloy-4 at High Stresses." *Materials Science and Engineering: A* 623 (2015): 114–123.

57. B. Kombaiah and K. Linga Murty. "High Temperature Creep and Deformation Microstructures in Recrystallized Zircaloy-4." *Philosophical Magazine* 95.15 (2015): 1656–1679.

58. J. E. Talia and F. Povolo. "Tensile Properties of Zircaloy-4." *Journal of Nuclear Materials* 67.1-2: 198–206, 1977.

59. H. Li et al. "Tensile Deformation Behaviors of Zircaloy-4 Alloy at Ambient and Elevated Temperatures: In Situ Neutron Diffraction and Simulation Study." *Journal of Nuclear Materials* 446.1–3: 134–141, 2014.

60. C. Liu et al. "Texture and Yielding Anisotropy of Zircaloy-4 Alloy Cladding Tube Produced by Cold Pilger Rolling and Annealing." *Materials Science and Engineering: A* 719: 147–154, 2018.

61. M. W. D. Cooper, C. Matthews, D. A. Andersson, *Gas Evolution in High-Burnup Fuel and Its Impact on Fuel Fragmentation*, LANL Technical Report for NEAMS, LA-UR-21-29789, 2021.

62. M. W. D. Cooper, C. Matthews, D. A. Andersson, *Development of Bubble Evolution Model for New Mechanistic Transient Fission Gas Release Capability in BISON*, LANL Technical Report for NEAMS, LA-UR-23-24769, 2023.

63. C. Galvin, D. A. Andersson, M. W. D. Cooper, *Demonstration of New Fracture Criteria Based on Micro-Structure and Compare to Empirical Model and Measurements*," LANL Technical Report for NEAMS, LA-UR-24-21606, 2023.

64. L. Holt, A. Schubert, P. Van Uffelen, C. T. Walker, E. Fridman, T. Sonoda, "Sensitivity Study on Xe Depletion in the High Burn-Up Structure of UO_2," *Journal of Nuclear Materials*, 452, pp. 166–172, 2014.

65. G. Pastore, L. Luzzi, V. Di Marcello, P. Van Uffelen, "Physics-Based Modelling of Fission Gas Swelling, Release in UO_2 Applied to Integral Fuel Rod Analysis," *Nuclear Engineering, Design*, Vol. 256, pp. 75–86, 10.1016/J.NUCENGDES.2012.12.002, 2013.

66. P. Hermansson and A. R. Massih, "An Effective Method for Calculation of Diffusive Flow in Spherical Grains," *Journal of Nuclear Materials*, Vol. 304, pp. 204–211, 2002. 10.1016/S0022-3115(02)00873-5.

67. K. Lassmann and H. Benk, "Numerical Algorithms for Intragranular Fission Gas Release," *Journal of Nuclear Materials*, Vol. 280, pp. 127–135, 2000, 10.1016/S0022-3115(00)00044-1.

68. G. Pastore, L. P. Swiler, J. D. Hales, S. R. Novascone, D. M. Perez, B. W. Spencer, L. Luzzi, P. Van Uffelen, R. L. Williamson, "Uncertainty, Sensitivity Analysis of Fission Gas Behavior in Engineering-Scale Fuel Modeling," *Journal of Nuclear Materials*, Vol. 456, pp. 398–408, 2015, 10.1016/J.JNUCMAT.2014.09.077.

69. G. Pastore, D. Pizzocri, C. Rabiti, T. Barani, P. Van Uffelen, L. Luzzi, "An Effective Numerical Algorithm for Intra-Granular Fission Gas Release during Non-Equilibrium Trapping, Resolution," *Journal of Nuclear Materials*, Vol. 509, pp. 687–699, 2018, 10.1016/J.JNUCMAT.2018.07.030.

70. T. Barani, G. Pastore, A. Magni, D. Pizzocri, P. Van Uffelen, L. Luzzi, "Modeling Intra-Granular Fission Gas Bubble Evolution, Coarsening in Uranium Dioxide during In-Pile Transients," *Journal of Nuclear Materials*, Vol. 538, pp. 152195, 2020, 10.1016/J.JNUCMAT.2020.152195.

71. T. Barani, G. Pastore, D. Pizzocri, D. A. Andersson, C. Matthews, A. Alfonsi, K. A. Gamble, P. Van Uffelen, L. Luzzi, J. D. Hales, "Multiscale Modeling of Fission Gas Behavior in U_3Si_2 under LWR Conditions," *Journal of Nuclear Materials*, Vol. 522, pp. 97–110, 2019, 10.1016/J.JNUCMAT.2019.04.037.

72. D. Pizzocri, C. Rabiti, L. Luzzi, T. Barani, P. Van Uffelen, G. Pastore, "PolyPole-1: An Accurate Numerical Algorithm for Intra-Granular Fission Gas Release," *Journal of Nuclear Materials*, Vol. 478, pp. 333–342, 2016, 10.1016/J.JNUCMAT.2016.06.028.

73. D. Pizzocri, G. Pastore, T. Barani, A. Magni, L. Luzzi, P. Van Uffelen, S. A. Pitts, A. Alfonsi, J. D. Hales, "A Model Describing Intra-Granular Fission Gas Behaviour in Oxide Fuel for Advanced Engineering Tools," *Journal of Nuclear Materials*, Vol. 502, pp. 323–330, 2018, 10.1016/J.JNUCMAT.2018.02.024

74. D. A. Andersson, P. Garcia, X. Y. Liu, G. Pastore, M. Tonks, P. Millett, B. Dorado, D. R. Gaston, D. Andrs, R. L. Williamson, R. C. Martineau, B. P. Uberuaga, C. R. Stanek, "Atomistic Modeling of Intrinsic, Radiation-Enhanced Fission Gas (Xe) Diffusion in $UO_{2\pm x}$: Implications for Nuclear Fuel Performance Modeling," *Journal of Nuclear Materials*, Vol. 451, pp. 225–242, 2014, 10.1016/J.JNUCMAT.2014.03.041.

75. D. A. Andersson, *Density Functional Theory Calculations of Defect, Fission Gas Properties in U-Si Fuels*, Los Alamos National Laboratory (LANL), Technical Report LA-UR-15-27996, 2016, 10.2172/1237246. http://www.osti.gov/servlets/purl/1237246/

76. C. K. C. Lieou, N. A. Capps, M. W. D. Cooper, P.-C. A. Simon, B. D. Wirth "An Integrated Statistical-Thermodynamic Model for Fission Gas Release, Swelling in Nuclear Fuels," *Journal of*

Nuclear Materials, Vol. 589, 2024, 154869, ISSN 0022-3115, https://doi.org/10.1016/j.jnucmat.2023.154869.

77. C. McKinney, R. Seibert, J. Werden, C. Parish, T. Gerczak, J. Harp, N. Capps, "Characterization of the Radial Microstructural Evolution in LWR UO_2 Using Electron Backscatter Diffraction," *Journal of Nuclear Materials*, Vol. 585, pp. 154605, 2023, 10.1016/J.JNUCMAT.2023.154605.
78. N. Capps, L. Aagesen, D. Andersson, O. Baldwin, W. C. Brinkley, M. W. D. Cooper, J. Harp, S. Novascone, P. C. A. Simon, C. Matthews, B. D. Wirth, "Empirical, Mechanistic Transient Fission Gas Release Model for High-Burnup LOCA Conditions," *Journal of Nuclear Materials*, Vol. 584, pp. 154557, 2023, 10.1016/J.JNUCMAT.2023.154557.
79. K. Lassmann, C. T. Walker, J. van de Laar, F. Lindström, "Modelling the High Burnup UO_2 Structure in LWR Fuel," *Journal of Nuclear Materials*, Vol. 226, pp. 1–8, 1995, 10.1016/0022-3115(95)00116-6.
80. L. K. Aagesen Jr, S. Biswas, K. A Gamble, W. Jiang, P.-C. A. Simon, B. W. Spencer, *Implementation, Testing of Physics-Based Pulverization Model in BISON,* Idaho National Laboratory, Technical Report INL/RPT-22-67941, 2022, 10.2172/1984930. https://www.osti.gov/servlets/purl/1984930/

APPENDIX A. BURNUP EXTNESION ACCOMPLISHMENTS

A.1 MULTIPHYSICS APPLICATIONS TECHNICAL AREA

The mission of the NEAMS Multiphysics Applications Technical Area mission is to use NEAMS tools to demonstrate capabilities and develop engineering-scale methodologies to expand the safe, reliable, economical operation of the existing nuclear fleet. A secondary objective is to identify capability gaps within the NEAMS tools and to work with other technical areas to address these gaps. The remainder of this section focuses on the engineering-scale efforts to develop a methodology to calculate FFRD susceptibility. Assumptions and capability gaps have been identified, and subsequent sections summarize efforts to illuminate the impact or lack of impact on the assumptions and gaps.

A.1.1 FULL-CORE LOCA DEMONSTRATION

Current nuclear reactor operating strategies limit burnup to a peak rod average of 62 GWd/tU, so NRC regulations and reactor technical specifications are not required to address safety-related concerns associated with high-burnup FFRD. The nuclear industry's intention to extend PWR cycle lengths and to increase the peak rod average burnup beyond 62 GWd/tU increases the probability for fuel to fragment, relocate, and possibly disperse during a LOCA event. Safety analysis tools have been developed and routinely deployed to ensure that the PCT of the hot rod remains below 1,204˚C with a 95/95 confidence level. These tools where not and have not been used to assess FFRD susceptibility to ensure plant safety, and at this time it remains unclear whether the existing industry and research tools can perform such an analysis. This assumption has resulted in an effort to evaluate core FFRD susceptibility. This effort assessed the important steady-state operational and fuel performance parameters known to contribute to FFRD susceptibility. The parameters were evaluated to inform future core design strategies intended to mitigate FFRD. Additionally, data on a subset of high-burnup fuel rods representing the high-burnup operation envelope were passed to TRACE for detailed thermal hydraulic evaluation and were subsequently passed to BISON for transient fuel performance analysis. Results from the BISON transient analysis were then used to determine cladding rupture susceptibility, parameters that increase rupture susceptibility, and FFRD susceptibility if rupture is predicted.

A.1.1.1 High-burnup steady-state analysis

A four-loop Westinghouse commercial PWR was chosen for this analysis. The reactor operates with an ambient pressure containment design and a total nuclear fuel assembly capacity of 193. Current fuel management strategies for the PWR leveraged for this work operated on an 18-month fuel cycle with a typical low-leakage "ring of fire" fresh fuel layout that uses low-enriched uranium fuel. Three burnup regions are typically used with 85–92 fresh fuel assemblies in the core interior surrounded by once-burned fuel assemblies, and mostly twice-burned fuel assemblies are on the core periphery, as shown in **Error! Reference source not found.**. The cycles are designed to operate continuously for approximately 500 effective full-power days. Details of reactor design and high-burnup core design are provided in the literature [1, 2].

Industry collaborators partnered with NEAMS to develop 24-month core design incorporating high-enrichment, high-burnup fuel. The core designs were developed using in-house methods proprietary to the industry collaborator. Two cycles were developed to transition from an 18-month to a 24-month core design. Subsequently, ten additional 24-month core designs were developed to reach an equilibrium pattern. It should be noted that these core designs did not meet all the necessary safety criteria and are intended to be representative for the purpose of this analysis. However, the results from this work are impactful and should be deemed conservative.

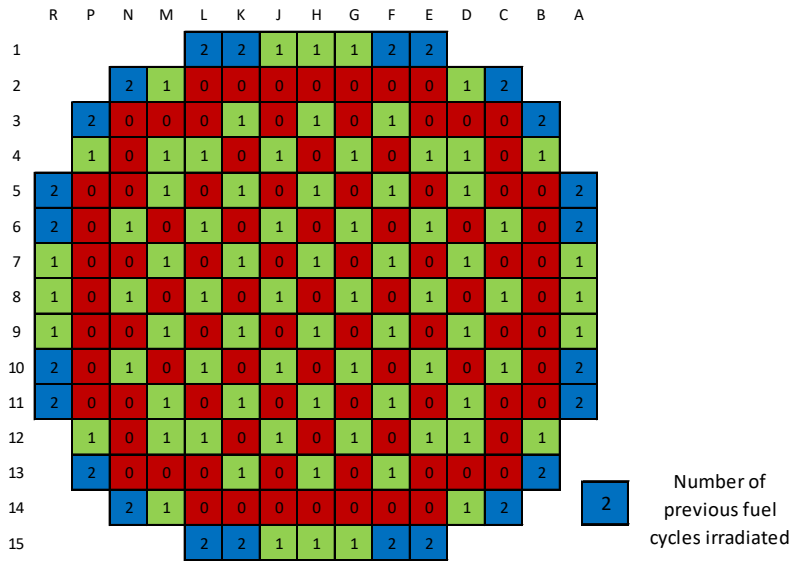

Figure 4. Standard 4-loop Westinghouse PWR core loading strategy.

The high-burnup depletion analysis used the core simulator tool, VERA, a state-of-the-art reactor analysis suite of high-fidelity software and methods capable of simulating the full operating history of a commercial PWR [14]. VERA includes advanced solvers and multiphysics coupling algorithms that provide the most rigorous solutions available today. VERA can accurately calculate the fuel rod and coolant conditions at very small spatial scales, including time-dependent isotopic depletion and decay, burnable poison depletion, and in-core detector response. VERA can also simulate local impacts of control rod movement and explicit effects of fuel assembly decay and shuffling that occurs during refueling outages. VERA has been applied to nearly ⅔ of the US commercial PWRs for simulation of over 200 operating fuel cycles [15,16].

all of the twelve core designs were implemented into VERA and depleted through the end of the cycle. The VERA-generated data were analyzed by considering the operating characteristics of interest to FFRD. Nine characteristics were considered and defined:

1. Average fuel rod burnup
2. Average fuel rod linear heat rate (LHR)
3. Average fuel rod decay heat production rate
4. Peak fuel rod burnup
5. Axial location of the peak fuel rod burnup
6. Local LHR at the axial location of the peak fuel rod burnup
7. Peak fuel rod LHR
8. Axial location of the peak fuel rod LHR
9. Local burnup at the axial location of the peak fuel rod LHR

Fuel rods in three final cycles were further downselected to eliminate those that did not achieve a rod average burnup of 62 GWd/tU by the end of the final cycle. Existing operational and safety limits were assumed to be adequate to address undesirable fuel performance behaviors in fuel rods with average burnups of less than 62 GWd/tU. Therefore, standard burnup fuel rods were not considered further in this work. Fuel rods inserted into the reactor before the first cycle under consideration were also downselected to eliminate those present during nonequilibrium operation, yielding 32,944 complete high-burnup fuel rod histories. The results of this analysis can be observed in **Error! Reference source not found.**.

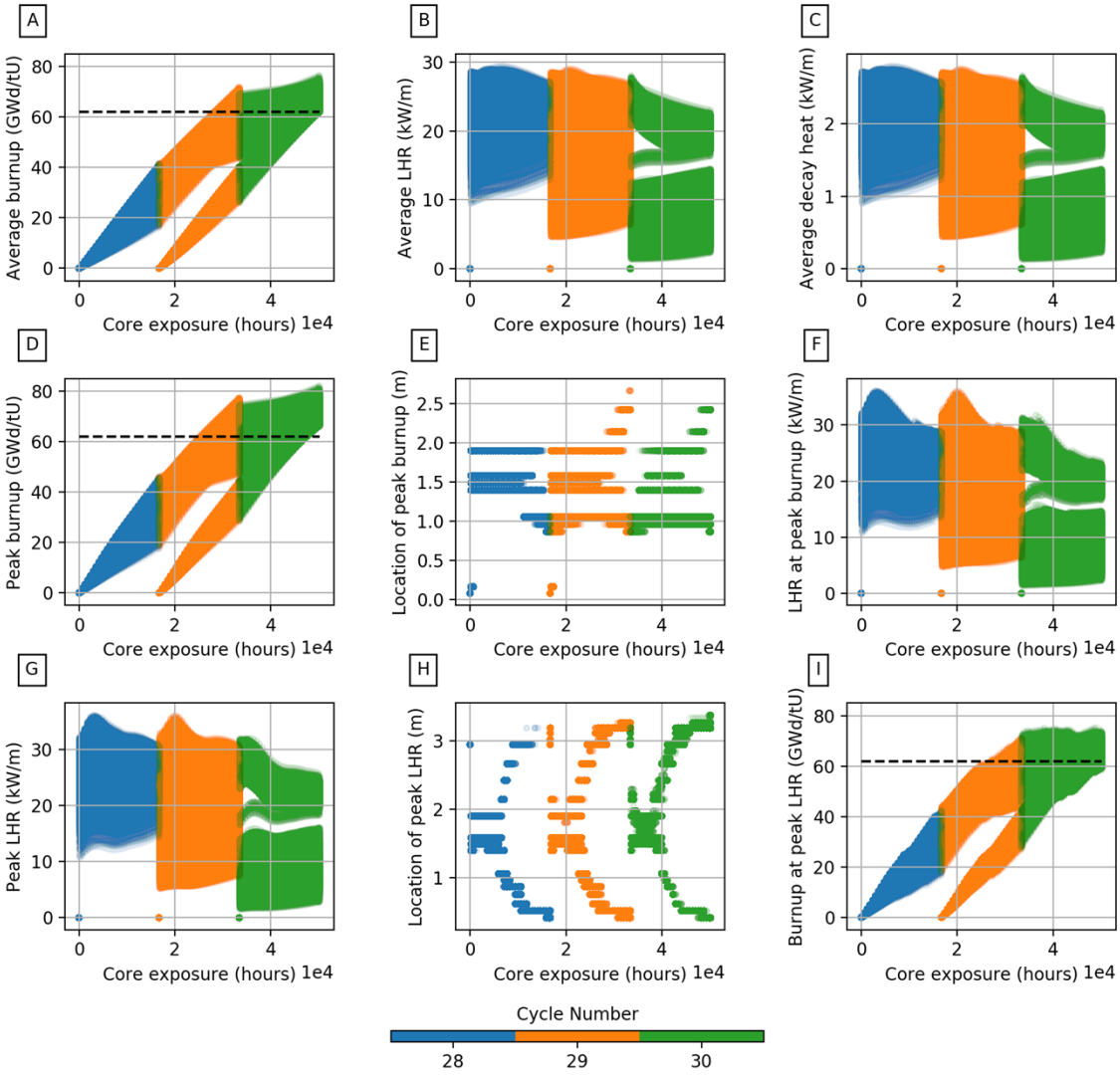

Figure 5. Time-dependent operating conditions extracted from 32,944 fuel rods irradiated in Cycles 28–30. Fuel rods irradiated in previous cycles and those that did not achieve an average burnup of at least 62 GWd/tU (marked by the dashed line) are not shown. The plots show that fuel rods experience wide ranges of operating conditions, which vary with fuel rod location and time.

Operating condition data from the 32,944 high-burnup fuel rods were sampled across all cycles and VERA depletion calculation states to calculate a set of statistics that describes the overall behavior of FFRD-relevant parameters for these core and fuel rod designs. The high-burnup cores provided by the industry partner leveraged a rotational quarter-core symmetry, and a symmetric geometric grid of 24 fuel rods per assembly was applied to the upper octant to select a variety of fuel rod locations with respect to both assemblies and the core. This process yielded 753 fuel rods which exhibited consistent statistics with the 32,944 high-burnup fuel rods. BISON was then used to evaluate key fuel performance characteristics as shown in **Error! Reference source not found.**.

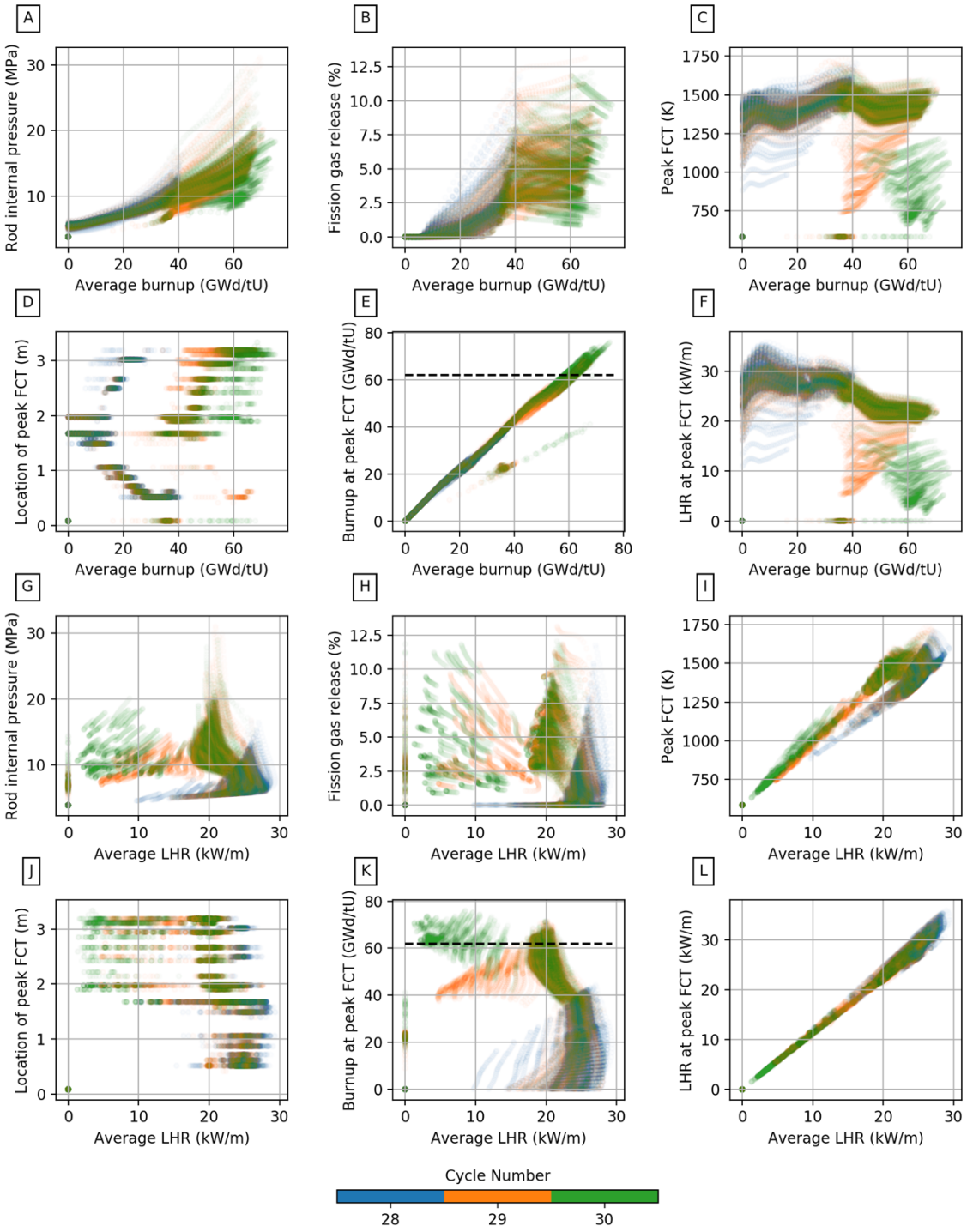

Figure 6. Average burnup and average LHR-dependent fuel performance results extracted from the 753 fuel rods selected for analysis in BISON. Opacity has been adjusted to show data that overlap in burnup and LHR spaces more clearly. Subplots A–C show that the fuel rods exhibit a wide range of responses to irradiation. Subplots D–L begin to illustrate correlations among fuel performance results and operating conditions

A.1.1.2 Transient thermal hydraulics analysis

The NRC's TRACE code was used to provide time-dependent cladding temperature conditions during the transient. TRACE was originally designed to investigate the PCT conditions for the hot rod and not for determining rod-by-rod cladding temperatures. The model used in this analysis originates from the TRACE distribution package used by the Best Estimate Methods, Uncertainty and Sensitivity Evaluation (BEMUSE) Organisation for Economic Co-operation and Development (OECD) International Benchmark VERA depletion, and BISON steady-state results were then used to provide input into TRACE.

BISON results were also compared with TRACE steady-state fuel temperatures of six bounding rods. The rods were selected based on power, burnup, and rod internal pressure, and finally, the hot rod was included. These rods were chosen to give a wide range of conditions for the BISON-TRACE comparison to provide confidence in TRACE's ability to accurately represent the pretransient fuel conditions. This comparison was extended to compare the fuel temperatures as a function of radius. An example of the temperature profile comparisons is shown in **Error! Reference source not found.**, which illustrates that the overall behavior was very similar, despite the local dips seen in the BISON profiles.

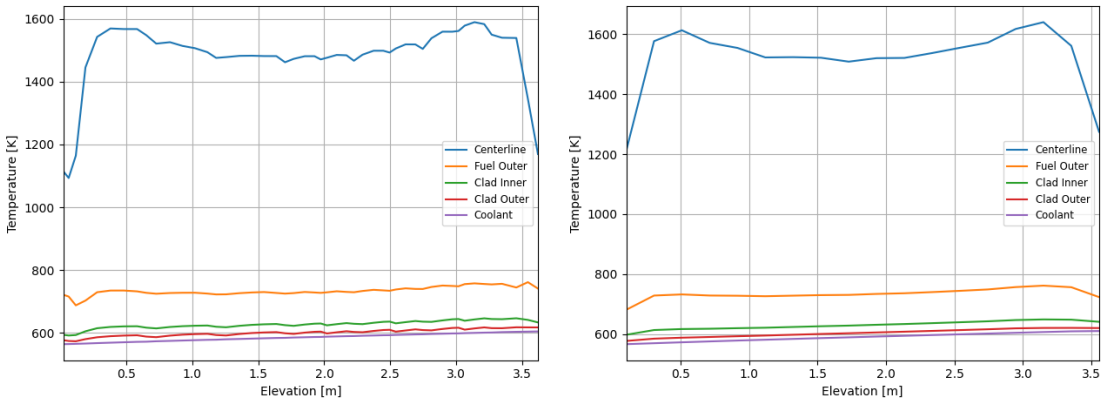

Figure 7. 2D steady-state rod temperature profile in BISON (left) and TRACE (right) for the maximum power high-burnup rod.

Results from subsequent analysis were used to further narrow the 753 rods down to 281 based on simply considering the time of the occurrence of the LOCA during the last high-burnup cycle. TRACE provided time- and spatially dependent cladding temperature results for all 281 high-burnup rods. The time-dependent PCT values for each rod are shown in **Error! Reference source not found.**.

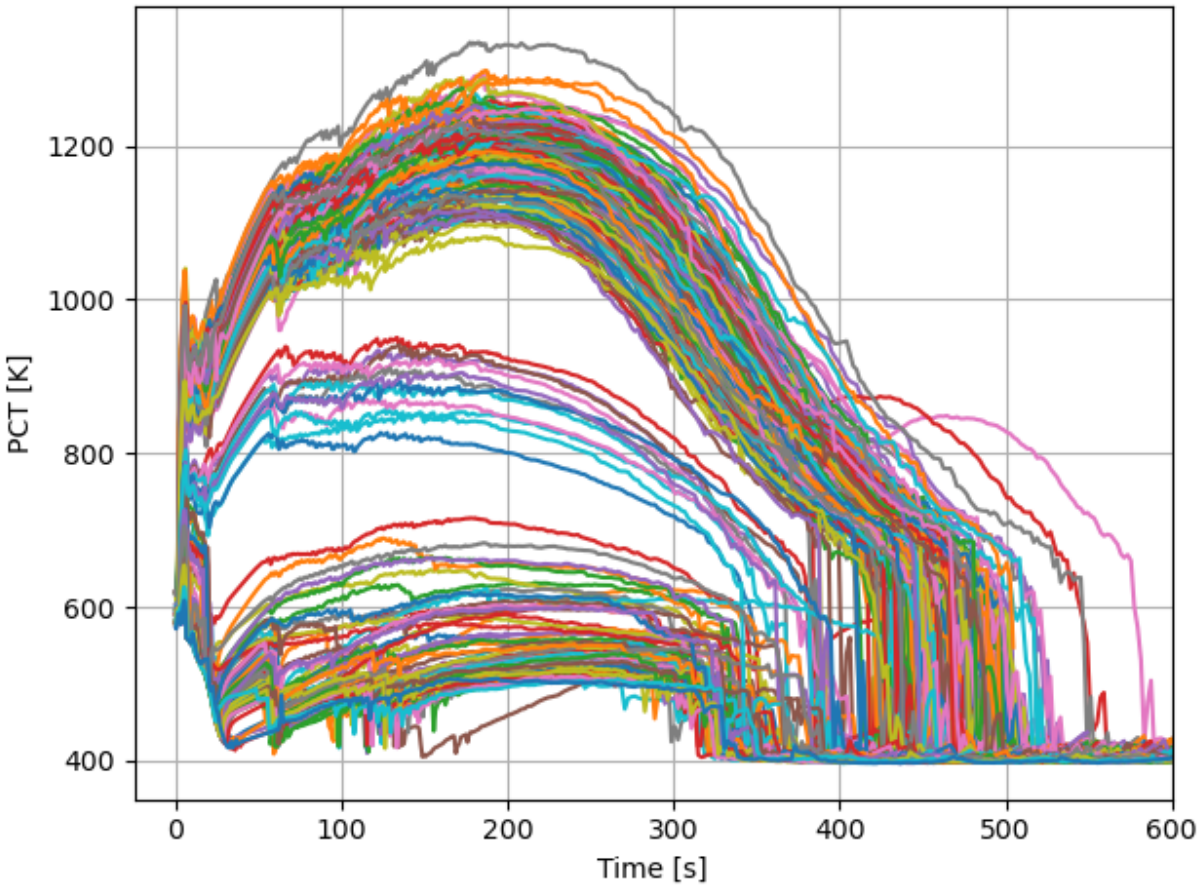

Figure 8. Large break LOCA PCT vs. time for the 281 selected high-burnup rods.

A.1.1.3 High-burnup fuel fragmentation relocation and dispersal susceptibility analysis

BISON was used to predict the transient fuel performance of the 281 high burnup rods. The steady-state BISON input files built by VERA were used as a starting point. TRACE results shown in **Error! Reference source not found.** were added as a boundary condition to the exterior cladding surface. Three different cladding failure models were considered in the analysis. The most conservative option for cladding failure was the Chapman correlation documented in NUREG 0630. **Error! Reference source not found.** shows BISON predictions for the once-burned rods delineating failed rods in red and non-failed rods in black. Second-cycle rods were considered in this analysis, but none of the examined rods experienced failure.

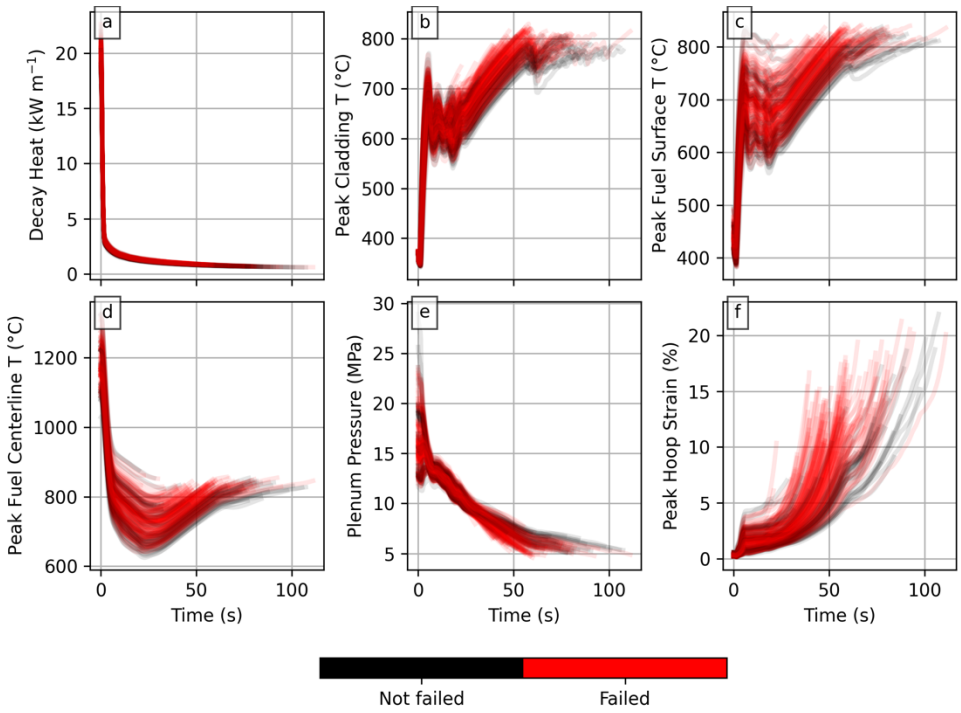

Figure 9. BISON predictions of fuel and cladding behavior of 203 high-burnup once-burned rods. Lines colors indicate whether the Chapman correlation predicted rod failure.

The BISON transient results presented here form the foundation for calculating the amount of fuel susceptible to being dispersed. The procedure used was as follows. First, determine the axial location where failure occurred using the cladding failure thresholds previously discussed. Second, determine the length susceptible to FFRD per the hoop strain threshold reported in the NRC RIL [5]. However, this work assumes that the mixing vanes and grid spacers will restrict FFRD to between the assemblies' structural components, so future work will investigate this assumption's applicability. Finally, the mass susceptible to pulverization can be estimated using correlations documented in the NRC RIL [5] or the Turnbull pulverization criteria 17]. **Error! Reference source not found.** summarizes the dispersal susceptibility analysis results.

Table 4. Summary of expected fuel dispersal based on (1) the NRC RIL correlation for particles less than 1 mm in diameter, (2) the NRC RIL for particles less than 2 mm in diameter, and (3) the Turnbull correlation.

	NRC RIL 1 mm	NRC RIL 2 mm	Turnbull
Average fuel susceptible to FFRD per failed rod (kg)	0.048	0.060	0.018
Total fuel susceptible to FFRD in simulated rods (kg)	7.35	9.18	2.72
Total fuel susceptible to FFRD in full core (kg)	330.9	413.7	122.4
Margin of error (kg)	±53.7	±67.1	±19.9

The following assumptions were made to complete the analysis:

1. tFGR was not considered in the transient analysis
   a. Potential impact → cladding rupture

2. Assembly structural features were assumed to prevent excessive relocation and dispersal
   a. Potential impact → relocation and dispersal susceptibility
3. Calculated cladding deformation
   a. Potential impact → rupture timing and balloon size (axial and hoop directions)
4. Pin-by-pin subchannel thermal hydraulics
   a. Potential impact → cladding temperature and rupture conditions
5. Rupture opening
   a. Potential impact → dispersal susceptibility
6. Empirical fragmentation criteria
   a. Potential impact → fragmentation relocation and dispersal

The results did not include the potential impact of double ballooning that results in failures in multiple axial locations, and although BISON did predict the formation of multiple balloons, the probability of multiple ruptures is low given the thermal hydraulic conditions and cladding performance during the LOCA.

A.1.2 Addressing Full-Core LOCA Modeling Assumptions

A.1.2.1 Empirical tFGR model and sensitivity study

Because the effect of tFGR was not addressed in the full-core simulation, BISON transient simulations were modified to include tFGR models. The effort is summarized here, but a more complete description is provided in the literature [18,19]. Three models were implemented in BISON: an empirical model, a linear model, and a built-in model.

The empirical model was developed from French tFGR data developed under the GASPARD program [20]. The data were fit to a double-sigmoidal function, which included parameters for the temperature (K), burnup (GWd/MtU), and heat rate (K/min), as indicated in Eq. (1):

$$tFGR(T,\beta) = \frac{100 - \frac{\beta^2}{f}a_2}{\left(1 + e^{\frac{-(T-x_1)a}{\beta b_1}}\right)^{c_1}} + \frac{\frac{\beta^2}{f}a_2}{\left(1 + e^{\frac{-(T-x_2)b}{\beta b_2}}\right)^{c_2}}, \#(1)$$

where *tFGR* represents the amount of FGR during the transient, T is temperature, β is burnup, and f, a_i, b_i, c_i, and x_i values were fit to the applicable experimental conditions, excluding the notched sample. Figure 4 shows the corresponding fits to the experimentally measured tFGR; the details of the model can be found in Capps et al. [19].

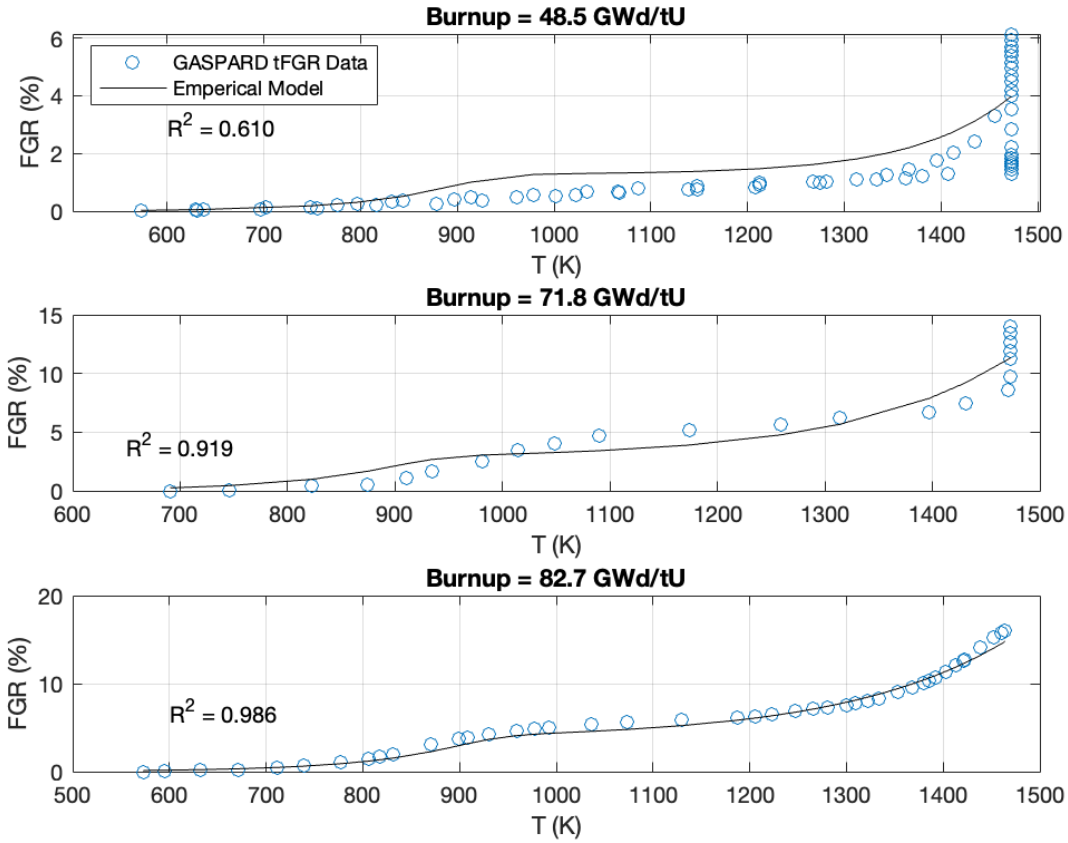

Figure 10. Comparison of optimal empirical double-sigmoidal tFGR fit presented in Eq. (1) (thin black line) compared with the single-pellet experimental data from the GASPARD program (open circles).

The linear model is described by Eq. **Error! Reference source not found.**,

$$FGR = \begin{cases} FGR_N, & t \le t_s \\ FGR_N + \dfrac{t - t_s}{\Delta t} p, & t_s < t < t_s + \Delta t, \\ FGR_N + p, & t \ge t_s + \Delta t \end{cases} \tag{2}$$

where FGR is the total amount of fission gas released, FGR_N is the nominal (i.e. nontransient) FGR, t_s is the transient start time, t is the current time, Δt is the time it takes for tFGR to occur, and p is the tFGR potential. p is defined as $p = (FGP - FGR_N)x$, where FGP is the amount of fission gas produced, and x is the fraction of fission gas released during the transient.

The linear model was not meant to be a realistic description of tFGR. Rather, it was meant as a tool to use when studying the sensitivity of BISON simulation predictions to the timing and amount of tFGR. Sensitivity studies work by selecting a set of baseline input parameters, changing those parameters one at a time, and then measuring the changes on the model outputs. Therefore, the sensitivity is the ratio of the relative change in the output to the relative change to the input. However, there is a large amount of uncertainty in x, the fraction of fission gas released during a transient. Therefore, multiple baselines were used. A single rod that failed according to both failure criteria used in the full-core analysis was selected for the study. Baseline release fractions of 0.75, 10, 20, and 50% were selected. The resulting sensitivities

for the 10% and 50% cases are shown in **Error! Reference source not found.** and **Error! Reference source not found.**, respectively. The Chapman correlation sensitivities tend to be very small, no matter the baseline. The strain rate criterion (SRC) showed a relatively high sensitivity of the hoop strain to the release fraction, but the direction of that sensitivity varied depending on the baseline release fraction. These results suggest that the behaviors are nonlinear and not easily extrapolated from one set of conditions to another.

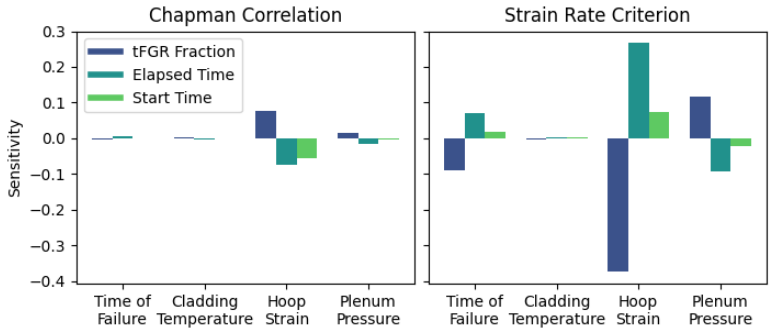

Figure 11. Sensitivities of rod failure characteristics to the linear model inputs when the baseline tFGR fraction is 10%.

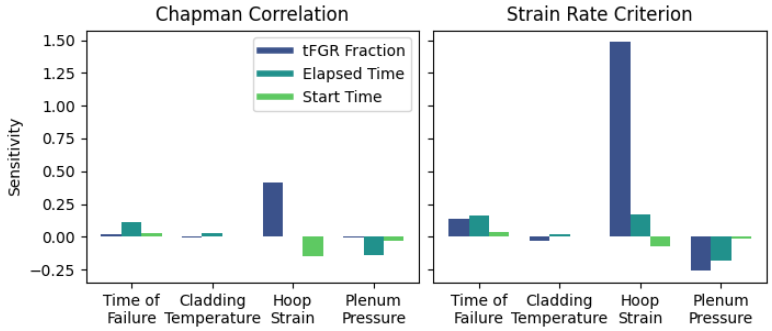

Figure 12. Sensitivities of rod failure characteristics to the linear model inputs when the baseline tFGR fraction is 50%.

The third model evaluated was a tFGR model already available in BISON that was developed by Barani et al. [21]. The model was applied to all 281 fuel rods modeled in the original BISON study. The times of failure for the nominal simulations are compared to the tFGR simulations presented in **Error! Reference source not found.**. The difference in the amount of fission gas released between the nominal and tFGR simulations is shown in **Error! Reference source not found.**. Both figures indicate that the effects of tFGR were relatively weak. The failure time changed only slightly, and the total change in FGR tended to be less than 1%.

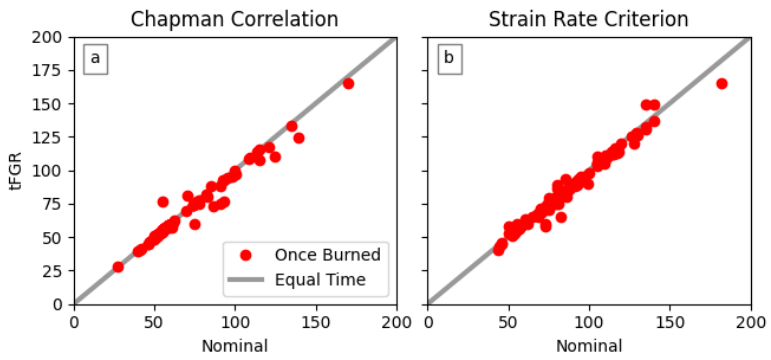

Figure 13. Comparison of the time of failure (s) between the nominal simulations and the corresponding simulations with the built-in tFGR model.

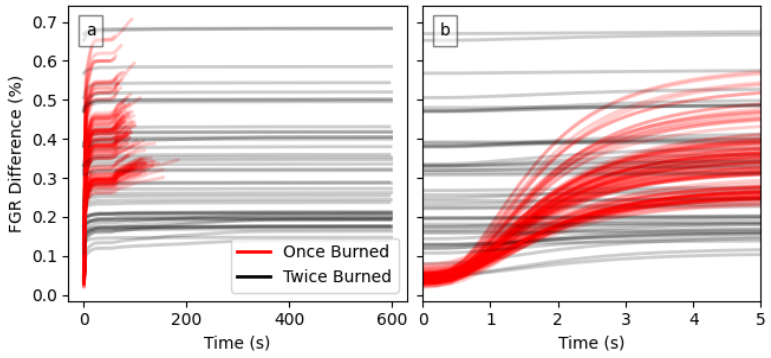

Figure 14. Change in FGR resulting from the inclusion of the built-in tFGR model: (a) full simulation time and (b) first 5 s of simulation time.

These simulations suggest that the uncertainty in model predictions associated with tFGR is much smaller than the uncertainty between the Chapman correlation and the SRC. Because the choice of cladding failure model will have a larger effect on FFRD predictions than the tFGR effects, tFGR model development is not need a high priority for near-term development.

A.1.2.2 Impact of assembly structural features

In the full-core LOCA analysis, it was assumed that the assembly structural features would prevent the cladding from ballooning beyond the cladding threshold outlined in the NRC RIL [5]. This assumption was built upon the knowledge that the assembly's structural features locally suppress power and in turn suppress local burnup. Additionally, the assembly's structural features are designed to promote cooling by mixing the working fluid (water or steam), and in the event of steam, the assembly is designed to disperse the entrained water droplets, thereby increasing heat transfer. All of these phenomena were considered in the depletion analysis and in the transient thermal analysis. When these conditions were applied in BISON, a local suppression of the cladding was seen where the assembly's structural features were located. Because the assembly structural features were not explicitly modeled in this analysis, the mechanical restraint was not fully captured. To address this gap, a BISON evaluation was used to validate the prevailing assumption that the assembly's structural features would locally suppress clad ballooning during a LOCA [22].

A.1.3 Simulation setup

The simulations presented in this section build on previous work, with an emphasis on evaluating the effects of structural features. Six spacer grids and three mixing vanes were added to the typical 2D RZ

fuel rod geometry. The geometry is shown in **Error! Reference source not found.**. **Error! Reference source not found.**a shows the plenum from a zoomed out perspective, **Error! Reference source not found.**b shows a spacer grid, and **Error! Reference source not found.**c shows the bottom of the fuel rod. The red colored block is designated as the fuel pellet stack, whereas grey is the cladding, and green is a spacer grid.

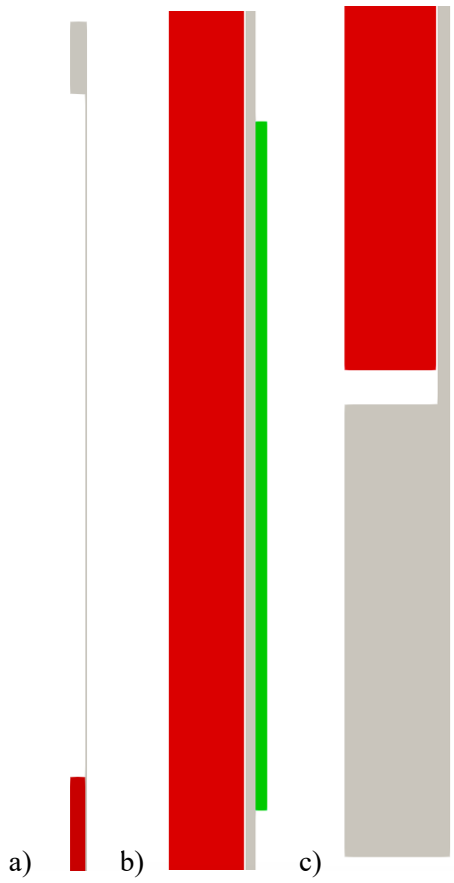

Figure 15. A representation of the 2D RZ mesh showing (a) the plenum, (b) the spacer grid, and (c) the base of the rod.

A 3D geometry was also considered and consists of a quarter full length rod with the same dimensions as in the 2D geometry. Specific boundary conditions were created to allow for the assembly's structural features to naturally deform while providing constraints based on the material's behavior on the outside of the cladding.

SIMULATION RESULTS

The assembly's structural features perform in a manner similar to that of a thicker cladding. This local behavior depresses clad ballooning in the areas where structural features are located. However, the adjacent areas of the cladding do not experience this depression, so they balloon and burst at similar times than seen in simulations without the effects of structural features. This behavior can be observed in **ERROR! REFERENCE SOURCE NOT FOUND.**, which presents a comparison of the cladding hoop creep strain with and without spacer grids for 2D and 3D simulations.

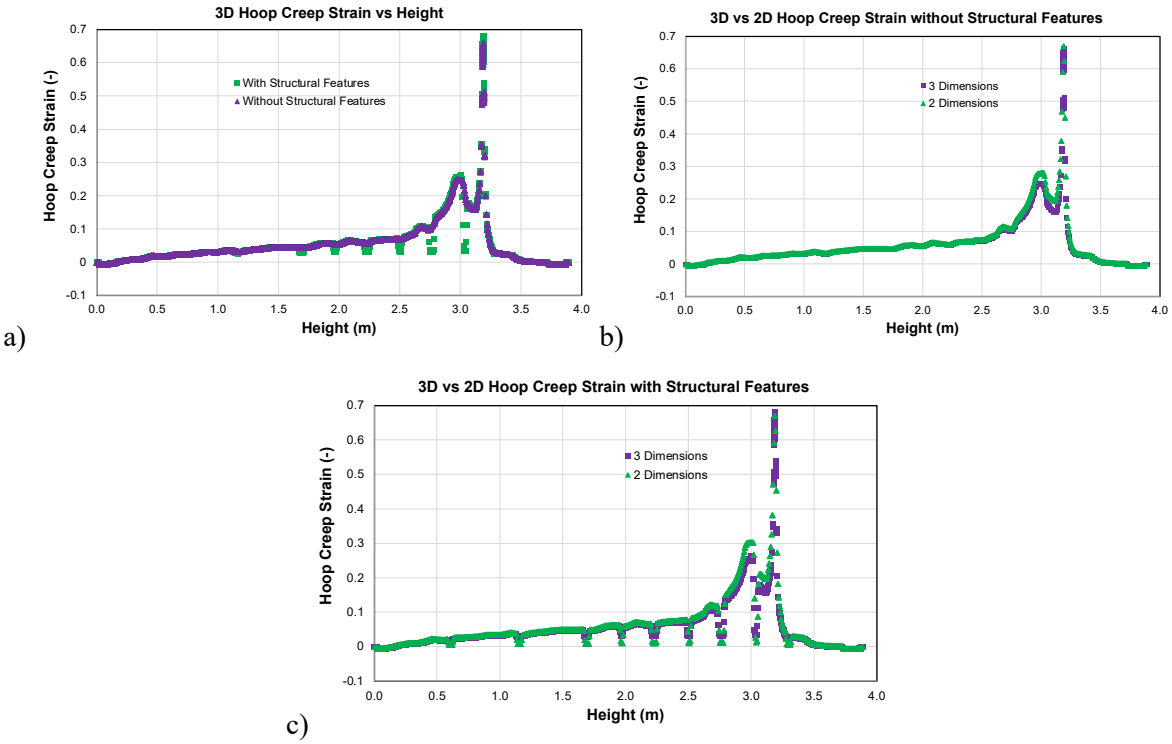

Figure 16. Hoop creep strain for the quarter rod at end of simulation with and without spacer grids (a) comparison of 2D and 3D results without grids (b), and (c) comparison of 2D and 3D results with grids.

The effect of the assembly structural features can be seen in the hoop creep strain plots at the local depressions axially along the cladding. However, balloon strain between the features remains unchanged compared to the simulation without structural features. This illustrates that fuel relocation following pulverization would be limited to the grid zones where rupture occurs. Finally, the assembly structural features appear to have a minor impact on the expected burst time.

A.1.4 Pin-by-Pin Subchannel Thermal Hydraulics

Accurate quantification of the thermal hydraulic behavior during LOCA is a critical aspect to consider when determining the risk of clad ballooning and FFRD. In a previous study on FFRD, RELAP5-3D was used to perform an LBLOCA analysis for a high-burnup core modeled using VERA [23]. The RELAP5-3D results were used as boundary conditions for BISON simulations of limiting rods in the core. The BISON simulations were then used to determine fuel pulverization susceptibility and the likelihood of fuel rod rupture in high-burnup fuel rods. A standard coarse-mesh two-channel pin modeling approach was used in the RELAP5-3D model in this analysis, which uses one pin and channel to represent limiting rods (high burnup and high power) and another pin and channel to represent the remainder of the elements.

In another activity, a TRACE model of a four-loop Westinghouse PWR LBLOCA transient [24] was developed. BISON was also used to assess high-burnup fuel FFRD susceptibility by analyzing fuel performance figures of merit such as rod internal pressure, FGR, PCT, and their relationships between one another and their dependencies on core location. The TRACE solution was used to provide boundary conditions for limiting pins modeled by BISON; however, a very coarse radial meshing approach was used that lumps assemblies in the core into five regions. Because of the effect of fuel rod performance gradients on FFRD susceptibility, it was determined that a study should be performed to investigate the

impact of significantly increasing the resolution of the thermal hydraulic solution so that every pin and coolant channel in the core is explicitly modeled using the CTF subchannel code [25].

A.1.4.1 Simulation setup

The four-loop Westinghouse PWR model that was used in a previous study on high-burnup cores [23] was used to determine the 3D core power distribution at the end of an extended cycle. **Error! Reference source not found.** shows the radial core burnup distribution at a selected level, with a black box surrounding 9 assemblies. Models were set up in both TRACE and CTF for this 9-assembly subregion. The TRACE model used one channel to model each assembly, and a CTF model was set up using the same approach so that the coarse CTF and TRACE models were as consistent as possible. The coarse models included two pins for each channel: one to represent the pin with the highest average power, and a second one to represent all the other pins. A second CTF model was created in which every pin and subchannel in the subregion was resolved, resulting in a more refined meshing.

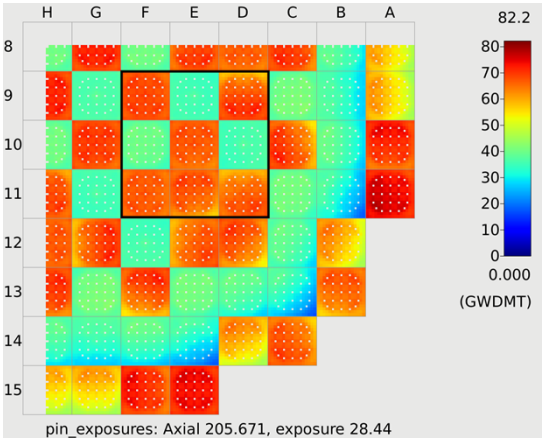

Figure 17. Burnup distribution in core at end of cycle and selected subregion for subchannel analysis of reflood transient.

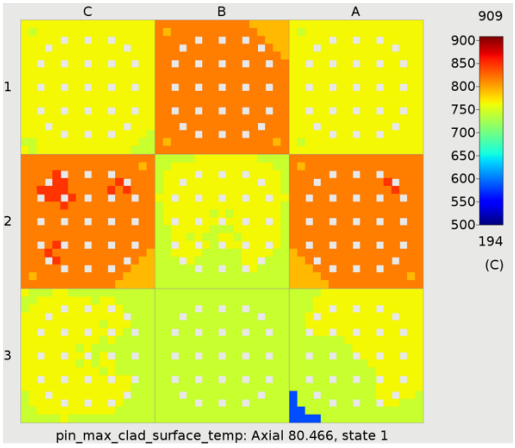

Figure 18. Radial distribution of initial pin temperatures in subregion for reflood transient (calculated based on initial pin power and TRACE results after blowdown and refill.)

The initial condition for the transient was 100% vapor. The initial pin axial temperature distribution was determined from a full TRACE simulation of the entire transient starting from the break, which explicitly resolved 324 pins. The pin axial temperature shapes were categorized based on the pin average power at the point where reflood starts. This relationship was used to set the pin axial temperature shape in the CTF and TRACE reflood models. The initial radial temperature distribution in the pin-resolved model is shown in **Error! Reference source not found.**. Boundary conditions include a 3.8 cm/s liquid reflood rate and outlet pressure of 2.5 bar. Average pin power was set so that a good match was obtained for PCT between the full TRACE system analysis and the TRACE subregion model.

A.1.4.2 Results

Error! Reference source not found. shows the transient clad behavior for all 9 assemblies in the subregion. The blue lines show the TRACE results, and the red lines show the coarse CTF results. The solid lines represent the hot pin results, and the dashed lines represent the lumped average pin results. The axial location where PCT occurs is shown for both models. The PCT occurs at different axial locations for each assembly and each pin, and the actual location is shown in the legend of each plot. The green shaded region represents the pin-resolved CTF model results. The axial location where PCT occurred in the

coarse CTF model is used to show the pin-resolved results. The pins experiencing maximum and minimum PCT are used for the bounds of the green shaded regions.

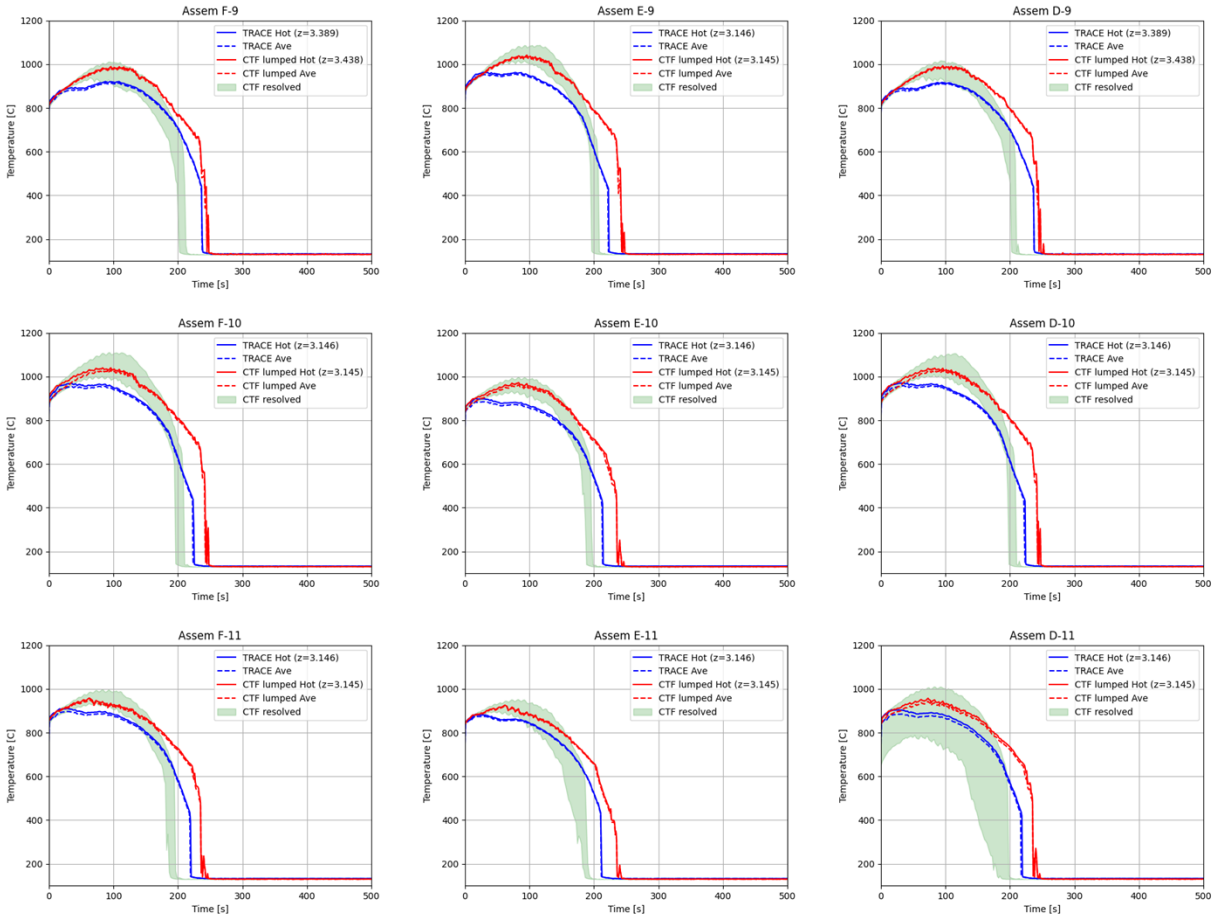

Figure 19. Transient clad surface temperature behavior during reflood in the 9 assemblies of the subregion model.

The lumped CTF model PCT always falls within the bounds of the pin-resolved results. The difference between the hot pin and average pin results in both CTF and TRACE lumped models is typically quite small compared to the range of clad temperatures in the resolved CTF model. It was observed that initial axial clad temperatures have a significant impact on transient clad temperature behavior, so it would be worthwhile to expand the CTF model to cover the full transient to obtain more accurate initial pin temperatures. Another observation is that PCT is always higher in the pin-resolved model, which is likely a result of the impact of capturing local thermal hydraulics. In other words, hot pins will communicate with hotter subchannels in the resolved model, whereas these details are lost in the coarse models. The pin-resolved results also have shown that the location of the most limiting pin is always different than the selected hot pin in the combined models because of the neighboring assemblies have much different power levels.

The resolved model also captures several pins with lower PCTs than the lumped model, which may be beneficial for gaining margin if the lower temperatures prevent burst. Even the lowest PCT pins in the resolved model are high and may be at risk of burst; however, a few points are noted. First, CTF is overpredicting PCT compared to TRACE, which may require further analysis of the heat transfer package being used. Second, the spacer grid models that capture spacer grid droplet breakup and spacer grid

quenching were not enabled in the CTF models because of current limitations of the CTF preprocessor used to build the model. Furthermore, the pin-to-pin radiative heat transfer model, which may have a significant impact on heat transfer between high- and low-burnup assemblies, was not enabled because of limitations of the preprocessor and lack of assessment. Enabling these additional models, improving on the LOCA validation base, and expanding on the model to include the full LOCA transient may result in a wider range of PCT values in the resolved model [29].

A.2 FUELS TECHNICAL AREAS

The NEAMS Fuels Technical Area develops advanced fuel performance models in BISON to support analysis of FFRD by utilizing a multi-scale materials approach to model fuel pellets and cladding. Specifically, the objective is to define improved models for the fuel fragmentation/pulverization threshold, tFGR, and cladding strain threshold that account for transient conditions and operational history while also resolving fuel and cladding chemistry and microstructure such that the models can be extended to address high-burnup issues and simulate new accident tolerant fuel concepts with relative ease. In addition, the Fuels Technical Area supports general capabilities in BISON to enable modeling of the operational history and condition of the fuel upon initiation of the transient event of interest for FFRD, tFGR, cladding ballooning, and failure simulations. Empirical models for FFRD are also implemented. The goal is to enable users to better bound current uncertainty related to these phenomena, to identify separate effects or integral experiments that can best assist fuel and cladding qualification efforts, and to facilitate interpretation of these experiments.

In the following sections, the BISON fuel performance capability is reviewed, followed by an overview of the cladding model development, including a description of how reduced order models are used to bridge the microstructure mechanical response to engineering-scale BISON simulations. This is followed by two sections addressing the microstructure evolution of the fuel pellet: (1) fission bubble evolution and impact on fragmentation threshold for individual grain boundaries, and (2) mesoscale simulations of grain restructuring and fracture simulations of the restructured grain structure accounting for the individual strength of boundaries as governed by grain boundary type, bubble population, and bubble state (pressure). The lower lengths scale work is based on two hypotheses. The first hypothesis states that the microstructural evolution during steady-state is fundamentally different in the colder periphery and mid-radius compared to the hot center as a result of atomic scale processes, which among other things lead to high-pressure fission gas bubbles. The second hypothesis is that the high-pressure bubbles drive stresses that result in the fuel fully (fragmentation/pulverization) or partially micro-cracking, breaking at the microscopic level, which governs fuel fragmentation and tFGR. Finally, the application of the advanced mechanistic models in BISON is demonstrated for cases in which the loop has been closed, such as better informed calculations for FGR fuel fracture. For cases in which this is still a work in progress, the status and outlook are discussed, including targeted benchmark and validation cases for advanced mechanistic models.

A.2.1 Fuel Performance Capability Overview

The BISON fuel performance code has an established framework and a myriad of capabilities to simulate steady-state fuel behavior for a variety of LWR designs and fuel-cladding systems resulting from years of program-funded development [38]. While development of many of these capabilities is ongoing, the process to change and add additional behavior and material models to simulate new conditions has been streamlined. Recent interest in extending BISON capabilities to meet reactor safety–relevant conditions has resulted in the addition and development of both empirical and physics-based material and behavioral models. This section provides a brief overview of the models being developed to extend the simulation of fuel behavior to encompass higher burnups and the subsequent implications on fuel rod behavior during a LOCA resulting from this increased fuel utilization. The specific models include high-burnup structure

(HBS) formation, fuel fragmentation, fuel pulverization, high-burnup FGR, high-temperature cladding creep, cladding failure, axial fuel relocation, axial gas communication, cladding oxidation, cladding rupture geometry, and fuel dispersal [31,32,33,34,35].

A.2.1.1 High-burnup structure formation

As fuel is irradiated to higher burnups, a rim begins to form in the periphery of the fuel characterized by an increased plutonium content, fission gas depletion in grains, increasing fuel porosity, and submicron grains [39]. This morphology change in the fuel leads to a reduction in the fuel's thermal properties within the rim region. The restructured volume fraction of fuel is calculated by using a relation from Barani et al. [30]. As the volume of the restructured fuel expands, the thickness of the rim region penetrates further into the fuel. This calculation informs the rim region's thickness and is coupled to the FGR model, as discussed below. To account for the fuel's increasing porosity, a correction factor was implemented into the thermal conductivity model which increases as the porosity increases [37].

A.2.1.2 Fuel fragmentation and pulverization

As thermal gradients arise in the fuel during the rise to full power, differential thermal expansion develops significant hoop stresses in the fuel which lead to fracture. Because these gradients are proportional to power, the number of fuel fragments produced also increases with power [40]. As more fragments are formed which are increasingly smaller, the propensity for axial relocation increases. To determine the number of fragments in the fuel, calculations are performed based on models by Coindreau [42], Walton [43], and Barani [44] which relate to the size of these fragments. These calculations are then used to inform the axial relocation model of the characteristic size of these fragments for a mass packing calculation.

A similar mass packing calculation is used by deriving the mass of fuel pulverized during temperature transients in high-burnup fuel. As the fuel increases in temperature, bubble over-pressurization leads to local stresses that fracture and subsequently pulverize the fuel [45]. This model uses the Turnbull threshold to determine the burnup and temperature limit for the fuel pulverization and a distribution of the fuel pulver sizes for the aforementioned mass packing fraction used in the axial relocation model. A mechanistic model is necessary to determine the actual bubble pressure arising in the fuel periphery to accurately determine the mass of fuel pulverized. A model is currently under development at Los Alamos National Laboratory and is described in detail in Section **Error! Reference source not found.**.

A.2.1.3 High-burnup FGR

A standard mechanistic-based FGR has been implemented into BISON for UO_2. This model, the simplified integrated fission gas release and swelling model (Sifgrs), calculates the amount of fission gas released based on diffusion, bubble concentrations, and interconnection of network grain boundary bubble. Using this framework, steady-state FGR is calculated [46]. To extend this model to high-burnup fuels under transient conditions, gas burst release models have been incorporated [37]. As fuel temperatures in the periphery of the pellet increase or decrease quickly, the resulting stresses in the fuel can lead to significant gas release. This is caused by microcracking or grain-face separation, which releases fission gas located on the fuel's grain boundaries. This model is currently under development, and the mechanistic underpinning of this model is described in Section **Error! Reference source not found.**.

A.2.1.4 High-temperature cladding creep

As cladding temperatures increase during a LOCA, the rod's internal pressure increases from increased FGR and thermal expansion of gas. As the stresses build in the cladding during heating, the cladding eventually begins to creep out because of the differential between the internal pressure and the reduced coolant system pressure. As the cladding creeps out, the rod begins to locally deform or balloon. This ballooned region serves as a volume to accommodate the relocated fuel mass, and, if local cladding failure occurs, then the balloon disperse the mass into the coolant system. To calculate the cladding creep strain to determine balloon geometry or cladding failure, creep models relevant at these high temperatures have been implemented into BISON [34]. These models utilize a rate-based phased change model to ensure that the creep behavior calculation is consistent with the cladding phase. Three high-temperature models have been implemented based on different experimental series conducted on Zircaloy cladding: Erbacher [48], Kaddour [49], and Donaldson [47]. Each of these models uses a similar Norton power-law creep format. Because of the limited experimental data used to generate these models and their lack of meaningful anisotropic behavior, a complete multiscale model is currently under development to fully define the cladding creep behavior space. As mentioned in Section**Error! Reference source not found.**, this multiscale model will allow for an accurate calculation of the cladding geometry and strain rate to better determine the amount of axial relocation which may occur and the cladding strain at failure.

A.2.1.5 Cladding failure

During the LOCA, the cladding deforms under high temperature and may rupture under the increased pressure loading. BISON contains three different criteria to determine cladding failure based on fundamental material failure modes:

1. **Stress-temperature criteria.** This failure criteria uses Erbacher [48] or Chapman [50] to determine a stress-temperature limit for cladding failure.

2. **Strain rate limit criteria.** This criterion uses a rough limit of the strain-rate [51] set to 2.78% per second. It is assumed that as the cladding reaches this strain rate, it is undergoing plastic instability and will rupture.

3. **Overstrain.** This criterion uses a rough limit of 33.6% engineering strain, if the cladding reaches the limit, then the rod is assumed to be failed. This criterion is developed from gross simplifications of phase- and temperature-specific cladding strain-at-failure data.

These models were developed using data from different experimental series, and, as such, they are best intended for their intended uses. As the mechanistic model for the cladding creep is further developed, it is expected that an improved cladding failure correlation will be developed.

A.2.1.6 Axial fuel relocation

As previously discussed, the fuel fragmentation and pulverization models each allow the calculation of the size and quantity of the loose fuel for a mass packing calculation. This calculation, in conjunction with a calculation of the volume in the cladding balloon region, allows for calculation of the mass of fuel eligible to relocate vertically in the fuel and the mass of fuel settled [32]. This calculation, based on work by Jernkvist and Massih, [41] discretizes the fuel into layers so that the calculations can be directly applied. By calculating the mass of fuel in the ballooned region of the cladding or in the regions above the

ballooned region, the mass of fuel susceptible to being dispersed at cladding rupture can also be calculated.

A.2.1.7 Cladding rupture geometry

The cladding rupture opening area is currently calculated by using the cladding hoop strain near the suspected burst location. By using the strain, the rupture opening length and width correlations can be used to determine the areal opening of the rupture for different opening shapes [31]. These are used to determine whether the fuel fragments and pulvers can escape through the opening. This model is not currently coupled to a dispersal model, although as more accurate cladding behavior is determined, opportunities for coupling this to a mass dispersal calculation may arise.

A.2.1.8 Fuel dispersal

Fuel dispersal from the cladding is calculated using the axial relocation model and cladding failure criteria. As the fuel relocates into the ballooned region of the cladding and the fragment size is determined, the dispersal criteria from the NRC RIL [5] may be used to calculate the fuel susceptible to dispersal. This model uses six criteria to calculate the mass of fuel released to the coolant based on the length of the cladding with hoop strains above a certain limit and the size and amount of fuel in the local area.

A.2.1.9 Fuel bonding and axial gas communication

During long irradiations, the fuel and cladding can chemically bond, effectively sealing the local region of the fuel and preventing the rod's internal gas to quickly equalize pressure across the rod span. In this situation, the cladding is more susceptible to bursting if the pressure increases in one of the sealed regions of the fuel by preventing the plenum to serve as a gas reservoir. However, the fuel–cladding bond also mitigates the cladding mechanical response (ballooning) by restraining deformation to some extent. As such, it is important to determine when the fuel and cladding is bonded, the strength of the bond, the permeability of the gas through the cracked fuel in the bonded region, and the pressure and mass of the gas in each region of the fuel rod. As a first step to a comprehensive simulation, a fuel bonding is currently under development to allow the fuel to adhere to the cladding after high burnups. Separately, a layered 2D approach was developed to allow gas communication for a discretized fuel rod [35].

A.2.1.10 Cladding oxidation

As cladding temperatures increase during a LOCA, the cladding begins to react with the steam in the pressure vessel. As the cladding oxidizes, the metal is consumed, and hydrogen gas is produced. An oxidation model is available which uses parabolic oxidation rates to be calculated based on several reported reaction rate kinetics. These types of models were developed by Leistikow [53], Cathcart-Pawel [52], and Prater and Courtright [54]. The oxidation model calculates the thickness of the oxide layer produced from the reaction and applies a thermal resistance to the cladding's exterior to simulate the thermal insulation of the oxide layer and the locally deposited energy from the exothermic reaction.

BISON contains capabilities to simulate high-burnup fuel behavior during a LOCA. Although many of these capabilities are still very empirical and limited in their application, mechanistic models are currently under development to extend simulation parameter space to these increased burnups. The subsequent sections of this chapter discuss and highlight the importance of these mechanistic models, the challenges associated with their development, and goals for their application.

A.2.2 Cladding Material Model Development and Application

A.2.2.1 Reduced order model development

The NRC RIL [5] notes that cladding performance has a direct impact on fuel dispersal susceptibility, and the full-core LOCA analysis identifies high-temperature cladding performance as a source of high uncertainty with respect the balloon geometry and rupture opening. Zircaloy is a complex alloy with hexagonal close-packed crystal symmetry at low temperatures which transitions to a body-centered cubic symmetry a high temperature. Similarly to all metals, performance variability will be inherently linked to variability in the initial microstructure of the material. To date, the envelope of Zircaloy performance cannot be quantified without onerous testing campaigns. The need for this type of analysis is exacerbated in the context of high-burnup and transient thermo-mechanical loading: in a LOCA scenario that occurs after the clad has been in service for a few months, the material will be damaged by the presence of irradiation-induced vacancy and interstitial clusters on distinct crystallographic planes and will likely see an increase in H content.

It is of the utmost importance to develop and validate models that can predict the performance variability of Zircaloy samples and structures under arbitrary loading scenarios and irradiation histories as a function of microstructure and dynamically evolving composition. Such an objective constitutes the primary goals of the proposed work. The strategy employed is original: to first develop and thoroughly validate a full-field polycrystal simulation tool that can predict the yield strength, ultimate tensile strength, minimum creep rate, creep rupture life, and irradiation creep of Zircaloy as a function of grain size, texture, precipitate content, H content, and dislocation content. This effort also aims to develop reduced-order constitutive models and to implement those into the MOOSE framework (**Error! Reference source not found.**). These surrogate models will reproduce the predictions from the polycrystal model and will critically maintain the ability to predict the mechanical response of the system under arbitrary loading scenarios. **Error! Reference source not found.** illustrates the approach proposed to derive these surrogate models.

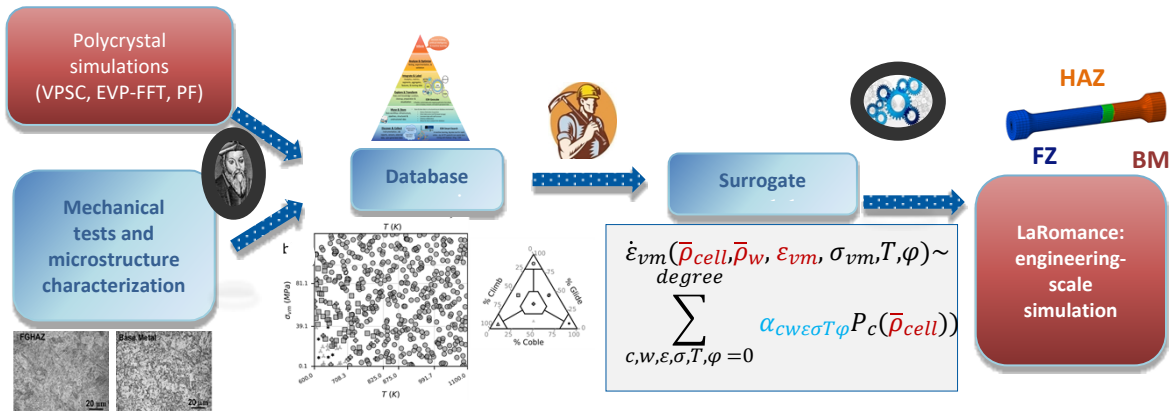

Figure 20. Methodology proposed to connect polycrystal simulations to structural finite element solvers.

Critically, the predictiveness of the surrogate models largely decays from the that of the polycrystal simulations used to generate the synthetic database. Over the past few years, a fast-Fourier-transform (FFT)–based full-field polycrystal solver known as Los Alamos Polycrystals (LAPX) was developed to predict the mechanical response of textured Zircaloy 4 samples. Note that the use of FFT enables generation of large synthetic databases of the expected response of the system. Critically, at each voxel within the sample, the model tracks the evolution of the relative and absolute contributions of dislocation glide, climb, and point defect diffusion to deformation. Furthermore, the model is also equipped with a homogenization method to track the effect of cavities on the magnitude and direction of plastic flow,

thereby enabling tracking of cavity evolution during thermal creep without empiricism. Development of such an advanced, general constitutive model necessarily entails the use of relatively large numbers of parameters. It is established that the link between properties and microstructures is not bijective such that several parameter sets could equally well predict the yield strength or other quantities (e.g., minimum creep rate) separately. To build trust in the ability of the model to extrapolate beyond calibration regimes, a unique parameter set was identified that simultaneously predicts all quantities of interest. **Error! Reference source not found.** illustrates the predictive capabilities of the model, showing that the model captures (a) the complex effect of temperature on yield strength, including the anomalous region between 400 and 550 °C, (b) the effect of stress and temperature on the creep rates (note that currently the model captures trends but is not yet sufficiently quantitative), (c) the effect of irradiation on swelling with an ability to predict the anisotropic growth observed experimentally, and (d) the effect of H on secondary and tertiary creep at multiple creep stresses. Note that validation data still lack for the latter use case.

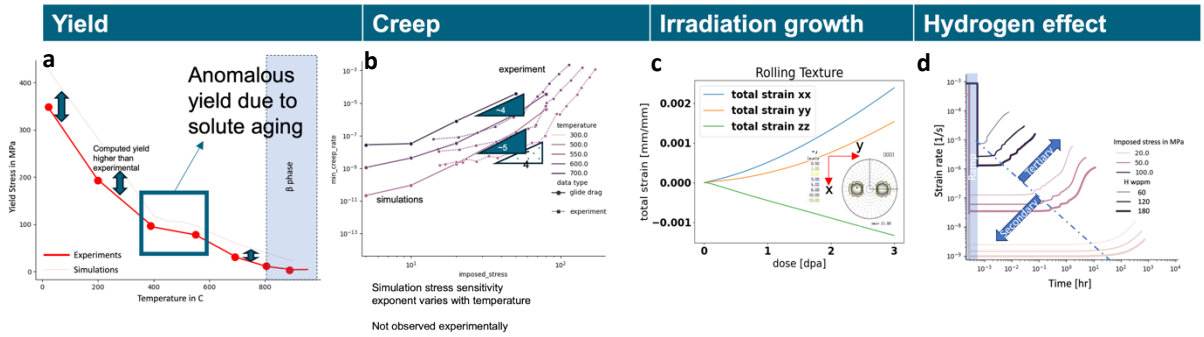

Figure 21. (a) Experimental and simulated yield stress [55] vs. temperature curve, (b) experimental and simulated minimum creep rate as a function of stress (between 5 and 150 Mpa and temperature between 500 and 600°C) [56,57], (c), irradiation growth strain in the principal direction vs. dose, and (d) simulated strain rate vs. time curves for multiple creep stress obtained by varying solid solution H content, from 60 to 180 ppm.

To further illustrate the subtlety and complexity of the problem, focus is placed on the case of the material's yield strength, in which these predictions show, in agreement with literature data, that tube-textured materials are stronger than plate-textured systems when loaded along the axial and rolling directions, respectively. The modest difference in yield strength of 10–20MPa can be translated into significant differences in the creep response, depending on stress and temperature.

As shown in LIGHT-WATER REACTOR STAKEHOLDER FEEDBACK(c), the complex temperature dependence of the yield strength is thought to be in part caused by the effects of solutes, leading to a preferential strengthening of the basal planes compared to the pyramidal <a> system vis a vis the basal system. These unexpected predictions are validated by predictions of the microstrains experienced by different crystallographic planes during loading. LIGHT-WATER REACTOR STAKEHOLDER FEEDBACK (d), shows simulations of virtual high-energy x-ray diffractions during tensile testing of Zircaloy plated along the transverse direction against experimental results [59]. Note that these experiments extract the average elastic strain within specific families of grains during testing. As shown, the subject model clearly predicts the magnitudes and the order of strain plane in agreement with experimental data.

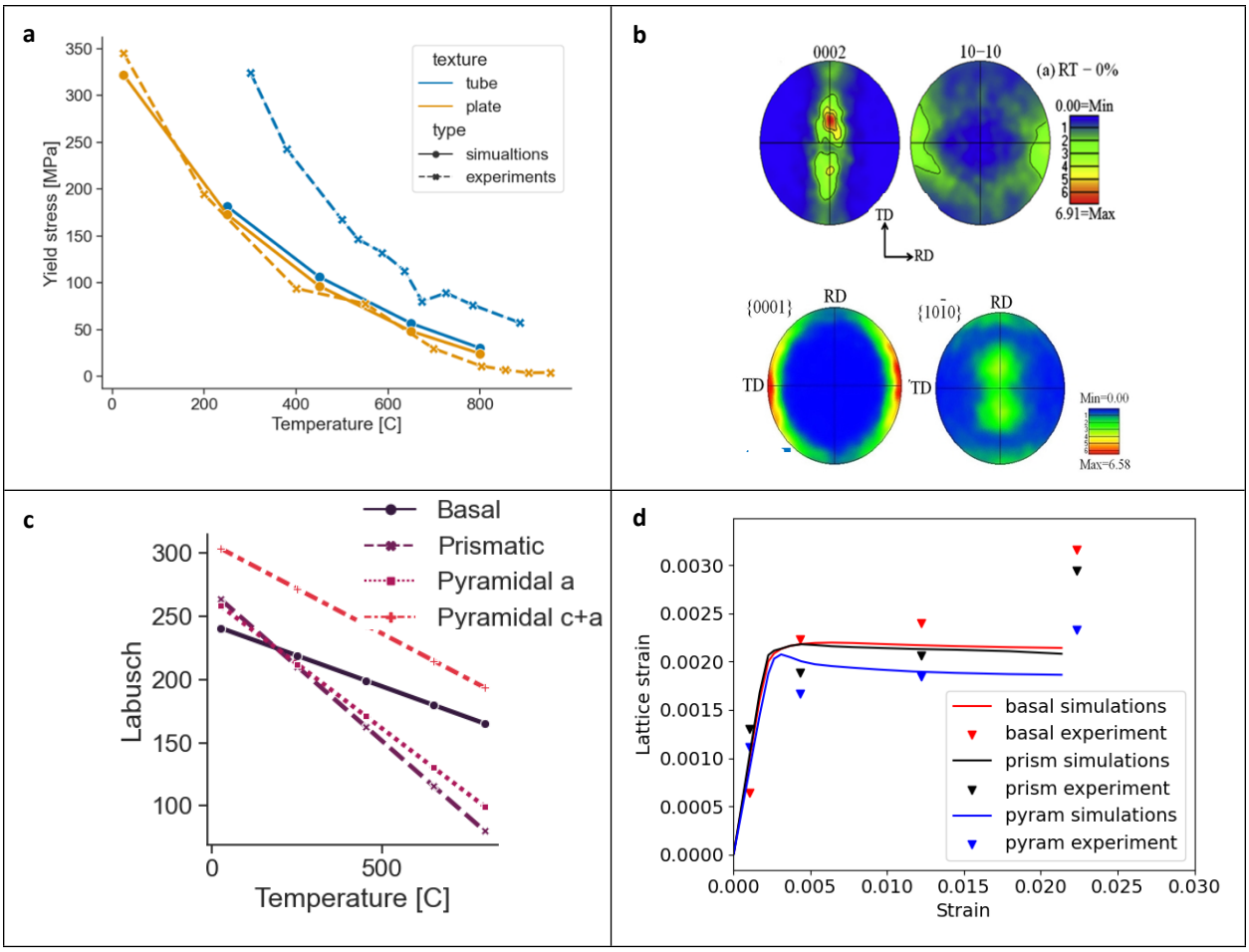

Figure 22. (a) Experimental and simulated yield stress vs. temperature curves for plate [55] and tube [58] samples, (b) basal (left) and prismatic (right) poles figure of a plate [59] (top) and tube (bottom) texture [60], (c) solute-strengthening contribution to the total friction stress of different slip modes, and (d) experimental [59] and simulated lattice strains at 250°C for a tensile test with an imposed strain rate of $1 \cdot 10^{-4}/s$.

A.2.3 Fuel Material Model Development and Application

A.2.3.1 Bubble over-pressurization, growth behavior, and fragmentation

Fission gas bubbles are thought to play a role in creating significant internal stress within the fuel microstructure that can lead to pulverization during a temperature transient. It is hypothesized that irradiation-induced defect processes drive bubble over-pressurization during reactor operation. Following this, a rapid increase in temperature drives thermal expansion of the gas in the bubbles leading to micro-cracking in the surrounding UO_2 matrix. This mechanism for release is distinct from the standard diffusion-based FGR and is termed *transient fission gas release* (tFGR). Furthermore, if the extent of the cracking is great enough, then the mechanical integrity of the fuel may be compromised, leading to fragmentation or pulverization. Fuel is particularly susceptible to pulverization in regions that have undergone restructuring, supporting the hypothesis that microstructural evolution under irradiation is a critical component governing the susceptibility to pulverize. This section summarizes the results of recent milestones using atomic-scale simulations to investigate (1) bubble pressure evolution during steady state [61,62], and (2) bubble-induced fracture during transients [63].

Bubble over-pressurization

The cluster dynamics code Centipede contains detailed information about a range of defects in UO_2 and solves for their concentrations and mobilities under irradiation. Centipede has been employed to simulate the arrival rates of defect at bubble [61,62]. Uranium will over-pressurize the bubbles by removing free space, and gas interstitials will over-pressurize bubbles by inserting more gas into that free space. Vacancies traveling by themselves or as component gas-vacancy clusters will enable an increase in the volume of the bubble, leading to depressurization. Hence, the formation of defects under irradiation and their mobility governs the rate at which they arrive at bubbles, thus governing bubble pressure evolution as function of time (see **Error! Reference source not found.**a). Critically, the mobility of these defects varies dramatically as a function of temperature, so very different behavior is anticipated for different positions in the pellet.

Error! Reference source not found.b shows the steady-state Xe-to-Schottky defect ratio of the bubble following cluster dynamics simulations. At low temperature, the bubbles reach very high Xe-to-Schottky ratios because of the irradiation-induced interstitial diffusion, whereas at low temperatures, vacancy diffusion lowers the Xe-to-Schottky ratio. Although the ratios are not exactly analogous to pressure, high Xe-to-Schottky ratios indicate over-pressurization, which may lead to microcracking, as discussed in the next section. Furthermore, the cluster dynamics simulations show that Xe interstitials dominate Xe diffusivity at low temperatures during irradiation.

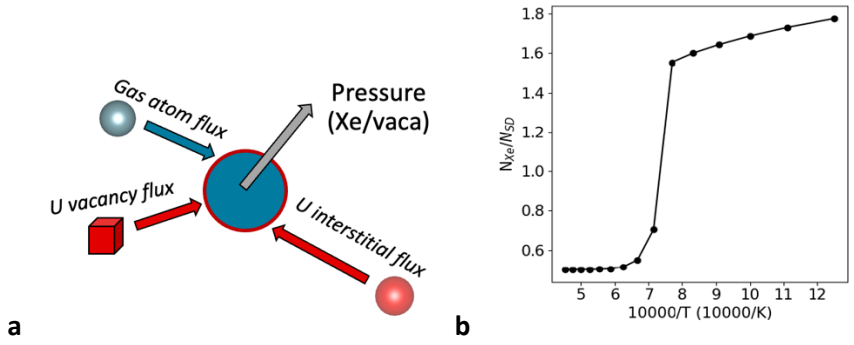

Figure 23. (a) Schematic illustration of the arrival of defects at a bubble evolving the bubble pressure, and (b) the steady-state Xe-to-Schottky ratio of the bubble as a function of inverse temperature predicted by cluster dynamics simulations.

Fragmentation at bubbles

Using molecular dynamics (MD), the mechanisms relevant to UO_2 fuel fragmentation [63] were investigated. Over-pressurized fission gas bubbles that form at grain boundaries in the high-burnup structure of UO_2 are believed to cause fuel fragmentation and pulverization after being subjected to a temperature ramp during a temperature transient. Additionally, this scenario can also cause tFGR in un-restructured fuel and in restructured fuel not at the pellet periphery. Therefore, an atomic-scale–informed model was developed to predict the pressure release mechanism for fission gas bubbles at grain boundaries. This model be implemented into longer length scale models. To discern the high pressures that bubbles at the grain boundaries could reach during steady-state operation Xe atoms were placed into a bubble located at a grain boundary, MD simulations were run at different temperatures, and the point at which the grain boundary begins to fracture was observed. A plot of pressure as a function of bubble diameter is shown in **Error! Reference source not found.**: the MD pressure release threshold at a grain boundary for different temperatures is indicated by colored lines.

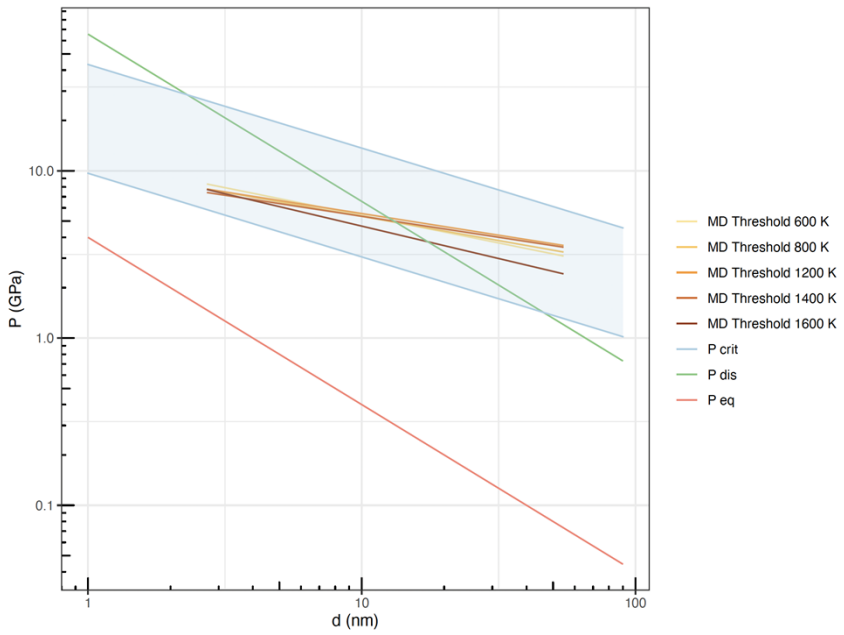

Figure 24. Plot of MD data showing how bubble pressure varies with diameter. Different pressure release mechanisms are indicated by the colored lines, where *P crit* is the pressure to crack in the bulk, *P dis* is the dislocation punching pressure, and *P eq* is the equilibrium bubble pressure.

Once bubble pressure was defined, temperature ramps simulating temperature transients for different bubble structures and initially at the atomistic informed pressure threshold were conducted, as illustrated in **Error! Reference source not found.**. This was accomplished by ramping different bubble structures from 600 K (the temperature at the periphery of a pellet) to higher temperatures. These results were then analyzed to predict the different criteria at which grain boundary fracture and grain boundary failure (complete separation of the grain boundary) occur. It was found that the initial separation between the bubbles influences the temperature at which the grain boundary fails. When the bubbles were placed closer together, grain boundary fracture occurred earlier, thus accelerating grain boundary failure at lower temperatures. All the bubble structures below the atomistic-informed pressure threshold had an initial pressure expansion when subjected to a temperature ramp, elastically deforming the UO_2 lattice. This pressure eventually became too high, causing the grain boundary to fracture to relieve the pressure.

Moreover, stress–strain MD simulations were carried out using the bubble structures from the temperature ramps in which the grain boundary did not fail to predict failure stresses at the grain boundary as a function of temperature and initial bubble separation. It was observed that for an increase in temperature, there is an associated decrease in the grain boundary failure stress. This is caused by the thermal expansion of the bubble, which assists in driving fracture. Furthermore, an increase in the bubble pressure also causes a lower failure stress, as well as a decrease in the initial bubble separation.

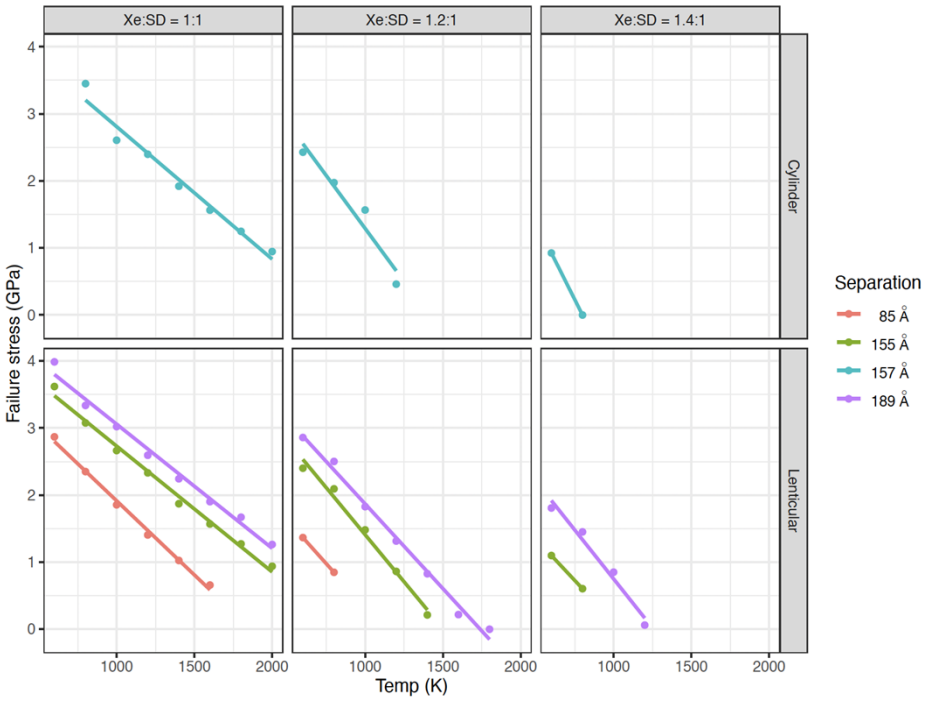

Figure 25. Failure stresses for a grain boundary containing a bubble at different temperatures, different pressures (Xe-to-Schottky ratio), and different bubble separations.

This information has been passed onto Idaho National Laboratory and was implemented into bubble their phase-field simulations examining bubble behavior in the HBS region during steady-state conditions and during a LOCA transient. These simulations are needed to inform the development of a mechanistic criterion for pulverization and fragmentation to be used in BISON. There are several assumptions which need to be made for the phase-field simulations and using atomistic simulations we aim to provide information to help parameterize these assumptions.

A.2.3.2 Mesoscale restructuring and fracture

The full core LOCA analysis and NRC RIL [5] make clear there is no applicable high-burnup FGR model under LOCA conditions. Similar, the current pulverization criteria are simply a fit intended to bound the available experimental conditions. With the inherent lack of available and applicable data, multiscale approaches like mesoscale codes aid in understanding restructuring, fission gas evolution, and pulverization within the HBS region. Incorporating the result from the previous section, this work couples phase field and cluster dynamics models to simulate the restructuring behavior and the associated fission gas evolution. The intragranular fission gas behavior is captured by the cluster dynamics model, whereas the microstructural evolution, including the evolution of grains and intergranular fission gas bubbles, is handled by the phase-field model. The cluster dynamics model accounts for the production, diffusion, clustering, and resolution of Xe within the grains. The phase-field simulation uses a grand-potential–based multiphase model to capture the evolution of the grain structure, along with the evolution of vacancies and gas atoms that lead to formation and growth of large intergranular bubbles. The model accounts for the restructuring of larger grains into smaller subgrains by introducing the new subgrains at a rate based on the energy associated with irradiation-driven dislocation accumulation.

Error! Reference source not found.shows different stages of HBS formation at 1,100 K (a temperature chosen for model testing at above-normal temperatures in the rim, but within the range of temperatures where HBS formation has been experimentally observed to occur [64]). The HBS formation initiates with

the formation of new grains around existing bubbles, triple junctions, and grain boundaries. The new grain formation is followed by the coarsening of the grains which proceeds inwards, eventually engulfing the as-fabricated damaged grains.

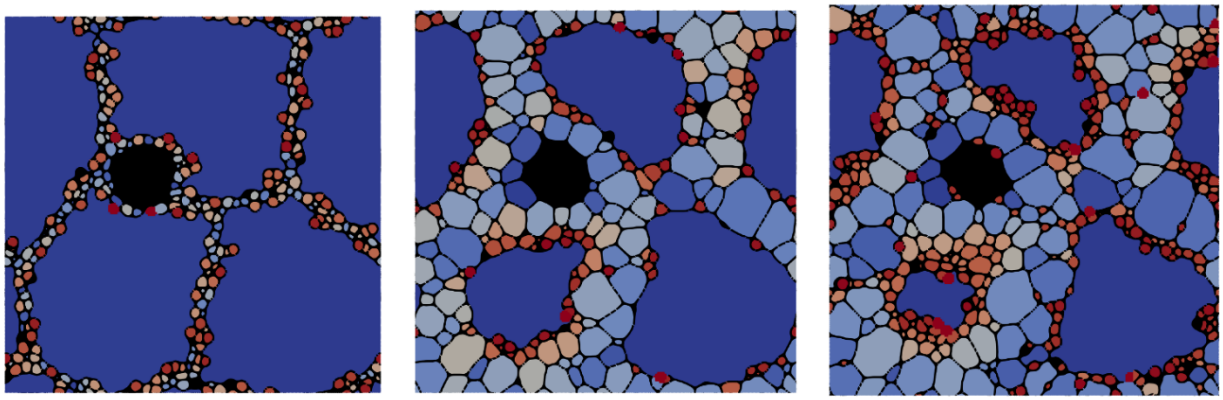

Figure 26. Different stages of HBS formation.

Error! Reference source not found.shows the morphology of bubbles with different initial sizes after growth at 1,200 K. In all the cases, growth of existing bubbles and formation of new triple-junction bubbles are observed. Additionally, the growth rate of the bubbles decreases with the increase in the initial bubble sizes. The model generates realistic HBS structures and bubble shapes similar to what has been observed experimentally.

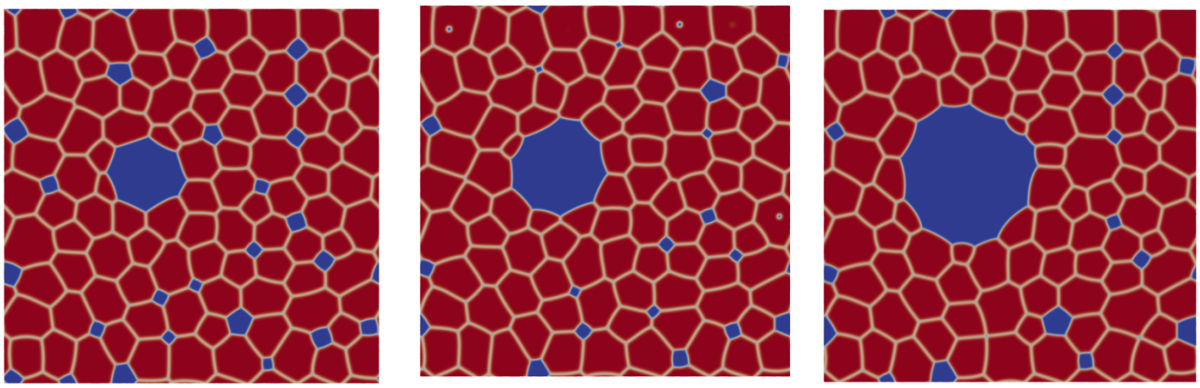

Figure 27. Bubble growth observed in fully formed HBS with initial bubble radii of 100 nm (left), 150 nm (middle), and 200 nm (right).

The generated microstructures have been used to analyze the pulverization criteria for the HBS using a phase-field fracture model. The model uses the critical fracture stress value calculated from the MD simulations mentioned above, accounting for the effect of temperature ramping and corresponding bubble pressure ramping during LOCA conditions to determine the pulverization criteria. **Error! Reference source not found.** depicts the fracture behavior in partially restructured HBS regions with varying restructuring fraction. It is observed that pulverization can occur at a restructuring fraction as low as 17%. Furthermore, for all the cases, the fracture occurs at similar bubble pressures and temperatures. It is concluded that the crack initiation is primarily governed by the bubble pressure, whereas the propagation is dictated by the weakened grain boundary networks. This mesoscale analysis provides inputs to the BISON model regarding the restructuring fraction and the critical bubble pressure at which pulverization occurs. The current effort focuses on extending the restructuring model to capture the grain subdivision observed in the inner region of the fuel known as the *dark zone*.

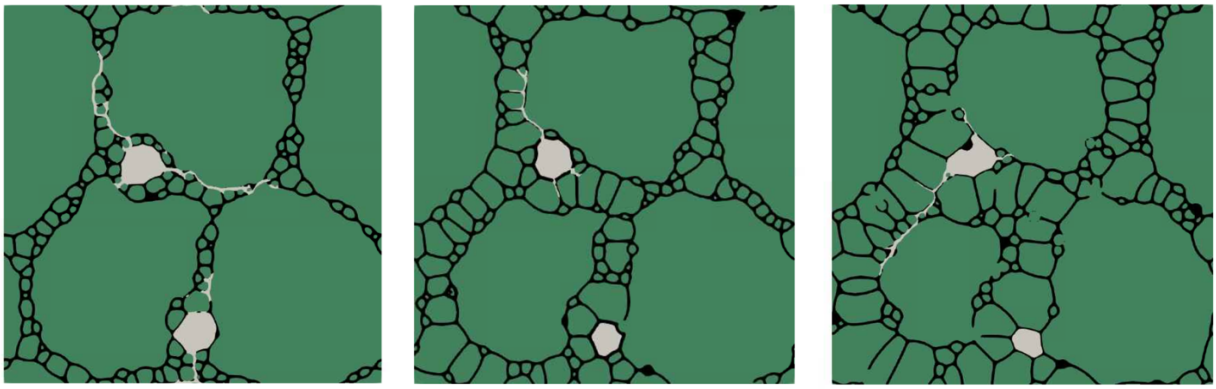

Figure 28. Fracture behavior in partially restructured HBS with 17%, 30%, and 45% restructuring with two bubbles.

A.2.3.3 Engineering-scale mechanistic model application

High-burnup burst FGR and fuel fragmentation and pulverization during a LOCA are not considered in traditional fuel performance modeling. Currently, steady-state and high-temperature fission gas behavior, release, and swelling are modeled in BISON using the state-of-the-art Sifgrs model [37]. Sifgrs employs a generally mechanistic approach to simulate fission gas behavior and describes different steps of fission gas transport and eventual release. It offers leading capabilities for intragranular fission gas modeling [65,73], describes intergranular fission gas behavior in the form of lenticular bubbles with coalescence criteria [65,71], and accounts for diffusional release and burst release caused by microcracking of fuel during temperature transients [2152]. Sifgrs leverages a mix of empirical, semi-empirical, and mechanistic models, including models informed by atomistic simulations [74,75].

At the start of this effort, Sifgrs did not offer burst FGR, high-burnup microstructural changes, or pulverization capabilities sufficient to support modeling high-burnup LOCA fuel performance. This gap was addressed through development of a mechanistic tFGR and fuel fragmentation model using the lower length scale efforts described throughout Section **Error! Reference source not found.** to directly inform engineering-scale fission gas modeling development. This multiscale, mechanistic approach alleviates some of the constraints imposed by the lack of available integral data and leverages microstructure and separate-effects data to validate the mechanistic components of the model. The sections below summarize how high-burnup behavior is modeled in BISON [37] and highlight how lower length scale efforts are incorporated into the engineering scale models.

A.2.3.3.1 Fuel microcracking during temperature transients

Sifgrs tracks several bubble populations: intragranular bubbles, intragranular bubbles pinned at dislocations, intergranular bubbles sitting at grain boundaries, and HBS bubbles. The growths of these populations follow different models, and each population contributes differently to fission gas behavior and release. Intragranular bubbles (pinned at dislocation or not) affect fission gas transport toward grain boundaries by trapping them. Intergranular bubbles collect fission gases once they reach grain boundaries and contribute to sudden FGR in two ways. First, once the surface fraction of intergranular bubbles reaches a given threshold, it forms a continuous channel that leads to FGR at free surfaces. Second, over-pressurized intergranular bubbles can result in grain boundary cracking and the subsequent release of the fission gas they contain, which is called *microcracking*. Note that microcracking is understood to be very local and does not result in fuel fragmentation. Microcracks have even been theorized to potentially heal, therefore restoring the grain boundary's ability to store fission gases. Microcracking was first described with an empirical model based on temperature transients, which was not explicitly tied to the mechanism

of grain boundary cracking at lower length scale [21]. More recently, a statistical-thermodynamic model was developed to describe microcracking as an energy-minimization phenomenon at the engineering scale, without insight from lower length scale simulations for grain boundary fracture behavior [76] (not yet available in BISON). Ongoing efforts rely on the work described in Section **Error! Reference source not found.**to accurately account for intergranular bubble growth, over-pressurization, and fuel microcracking. Once completed, BISON users will have a multiscale, mechanistic model alternative to the empirical model first implemented by Barani et al. [21] for fuel microcracking during temperature transients.

ç High-burnup fuel performance and fission gas behavior

As the nuclear industry's drive to extend burnup beyond current licensing practices grows to optimize fuel utilization, the need to understand high-burnup fuel performance becomes crucial. However, at high burnup, fuel performance and fission gas behavior are strongly impacted by important microstructural changes. The formation of HBS on the pellet rim and of a dark zone around the pellet center is characterized by formation of smaller grains and the emergence of a higher bubble density [77]. These microstructural changes affect fission gas behavior and enable new mechanisms for FGR, especially during transients [5,78].

Two models are currently available in BISON for HBS formation. The first model is an empirical description from Lassmann et al. [79] which states that the fuel immediately turns to HBS once burnup reaches a threshold value (between 55 and 70 MWd/kgU). Barani et al. later developed a more descriptive model for HBS formation [30] that predicts that the volume fraction of HBS evolves as follows:

$$\alpha = 1 - \exp\left(-K\, bu_{eff}^{\gamma}\right),$$

where $K = 1.52 \times 10^{-7}\ (MWd/kgU)^{-\gamma}$, the transformation rate constant; $\gamma = 3.54$ (-), the Avrami constant; and bu_{eff}^{γ}, the effective local burnup (accumulated burnup below 1,273 K). The model from Barani et al. therefore accounts for a gradual transition from nonrestructured fuel to HBS, with a limited effect of temperature in the effective burnup to prevent HBS formation in high-temperature fuel. However, the kinetics of HBS formation are independent of temperature and do not account for the initial fuel microstructure, and they also do not describe the actual mechanism for HBS formation. To better understand HBS formation mechanisms and account for microstructural and temperature effects, ongoing efforts are leveraging the mesoscale work presented in Section **Error! Reference source not found.**to describe HBS formation.

As HBS forms, which is characterized by subgrain formation, fission gases are quickly collected by subgrain boundaries and diffuse toward HBS bubbles. Newly generated fission gases appear in the HBS matrix (the inside of the grains) and diffuse toward grain boundaries and collect in HBS bubbles. This behavior was recently implemented in BISON, and the results of a test case are presented in **Error! Reference source not found.** [37]. Ongoing work is focusing on validating the model.

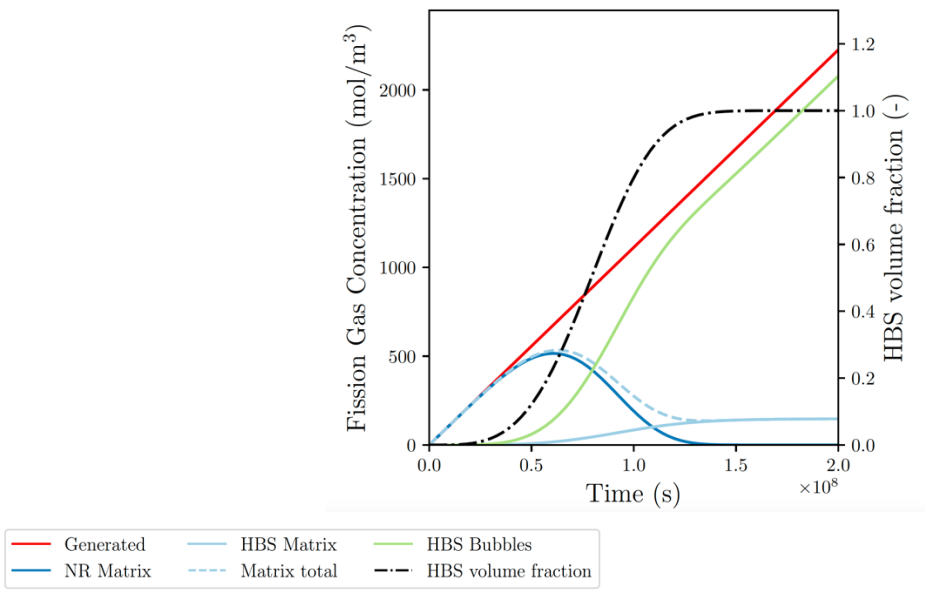

Figure 29. Fission gas behavior during HBS formation (NR = nonrestructured fuel) [37].

One of the main mechanisms for FGR during a temperature transient at high burnup is hypothesized to be HBS pulverization, which creates additional free surfaces for fission gases to be released. A rudimentary empirical model was proposed by Jernkvist and Massih [36]. In addition to this model, BISON leverages mechanistic lower length scale efforts as detailed in Section **Error! Reference source not found.** to obtain a physics-informed criterion for the onset of HBS pulverization. Above a HBS volume fraction threshold informed by lower length scale calculations, the HBS bubble pressure is compared to a critical HBS bubble pressure, itself informed by mesoscale fracture models. Pulverization occurs when the HBS bubble pressure is above the critical pressure and the fuel is broken down into fragments of a set size based on experimental measurements of fragment sizes [80]. The release caused by pulverization is then derived based on HBS porosity and the bubble size–to–fragment size ratio based on microstructural considerations. The amount of fission gas released via HBS pulverization n_{FG}^{pul} is defined as follows [80,37]:

$$n_{FG}^{pul} = f_V^{pul} V_b^{pul} n_{FG}, \tag{3}$$

where V_b^{pul} is the bubble volume in pulverized fuel, $n_{FG}$is the amount of fission gas in HBS bubbles, and

$$f_V^{pul} = c_p p + c_r \frac{R_b}{l_f} + c_0, \tag{4}$$

where c_p = 0.03 (-) is the coefficient for the porosity, c_r = 5.17 (-) is the coefficient for the bubble-radius-to-fragment-size ratio R_b/l_f, and c_0 = 0.02$ (-) is a constant [80,37]. This rudimentary but mechanistic model for FGR due to HBS pulverization is currently being benchmarked against the empirical model from Capps et al. [78] (see **Error! Reference source not found.**) and validated using experimental data.

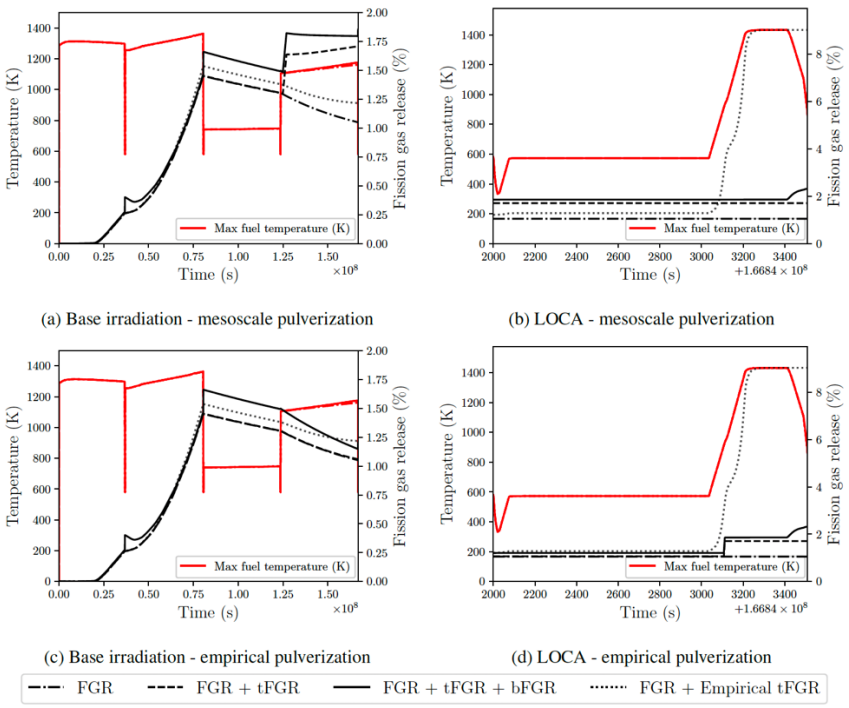

Figure 30. Comparison of the FGR predictions from the purely diffusional model (FGR), the mechanistic FGR model (FGR + tFGR), the mechanistic model with the microcracking burst model (FGR + tFGR + bFGR), and the empirical model (FGR + Empirical tFGR). Results for base irradiation (a, c), the LOCA scenario (b, d) results using the mechanistic multiscale pulverization model (a, b), and show results for the empirical pulverization model [36,37].

Preliminary results such as the benchmark results shown in **Error! Reference source not found.** seem to suggest that the current model underpredicts the amount of FGR during transients. This is attributed to the fact that this model only accounts for contributions from the HBS region, or the pellet rim, whereas extended fuel cracking and fragmentation are also observed in the dark zone region [77]. Ongoing efforts are focused on modeling dark zone formation and its impact on fission gas behavior, but very limited experimental data are available. As a result, BISON will leverage mesoscale investigation of potential mechanisms for dark zone formation.

A.3 THERMAL HYDRAULICS TECHNICAL AREA

Based on previous activities investigating the impact of thermal hydraulics on FFRD risk, it was determined that a study was needed to analyze the impact of using a higher resolution subchannel approach when modeling LOCA. Although NEAMS has the CTF capability, which includes models for LOCA conditions, these models were assessed before the software was adopted by the NEAMS program. Because of this, it was determined that an assessment of these models was required before CTF was used for this application.

A.3.1 Approach

The FEBA experiments were performed in the 1980s to measure rod bundle behavior during the reflood portion of a LOCA transient [26]. The data from these tests are openly available and include clad surface temperature measurements at multiple locations, as well as measurements of experimental housing temperature, fluid temperature, droplet carryover, and pressure drop. The rod bundle is a 5×5 lattice roughly 4 m high, and it includes spacer grids with an axial spacing of 545 mm. All electrically heated

pins are of the same dimensions, having an outer diameter of 10.75 mm. The same cosine-shaped axial power distribution is used in all pins. A thick 6.5 mm housing surrounds the bundle, which acts like surrounding pins and helps to simulate a larger rod-bundle lattice.

Two cases from these experiments were modeled: a low flooding rate case (3.8 cm/s) and a high flooding rate case (5.8 cm/s). Both cases have an outlet pressure of 4 bar, and their inlet temperatures are similar, varying between 37 and 53°C. The total bundle power was set to mimic decay heat according to the 120% American Nuclear Society (ANS) standard 40 s after shutdown. Models were set up in both TRACE and CTF. The CTF models included both coarse and resolved variants. The TRACE and coarse CTF models both used one channel for the bundle and a single pin to represent all pins. The resolved CTF model was a ⅛ symmetry model that captured all subchannels and pins individually. The same axial mesh was used in all models.

In addition to obtaining a baseline assessment of CTF LOCA capabilities with this activity, several issues were found and fixed in the code as needed for the core-scale demonstration. These fixes included model corrections and numerical stability improvements.

A.3.2 Results

Error! Reference source not found. shows the transient clad surface temperature prediction at 8 different locations. The subfigures are shown in order of increasing axial location in the bundle. The CTF coarse model results are indicated by the red line, the TRACE coarse model results are indicated by the blue line, the resolved CTF results are represented by the green line, and the dashed black line indicates experimental results. The resolved model is observed to overpredict the PCT in all upper locations of the bundle. When considering individual pin behavior, the interior pins were found to be significantly hotter than the periphery pins in the pin-resolved model. This may be caused by a lack of mixing, but it is more likely that the solid-to-solid radiative heat transfer model being disabled is causing insufficient radial heat transfer. This complex model has not been suitably assessed in time for this activity, so it was not enabled. The lumped models are not negatively affected by a lack of this model because radial heat transfer is already instantaneous because there is only one channel.

Otherwise, the results using the lumped CTF and TRACE models are generally in good agreement with each other and with the experimental data in terms of PCT. The exception is the upper portion of the bundle, which is overpredicted by both codes, but by a larger degree in CTF. A study was conducted to investigate the impact of the spacer grid droplet breakup and quenching models using the best estimate of spacer grid parameters, and it was found that this drops the PCT of the CTF models to be more in line with the TRACE results. The quench time is usually earlier than experimental results in both codes. It was shown that this could be caused by insufficient quench front entrainment. Comparison against droplet carryover shows that CTF may be underpredicting entrainment. If this issue were resolved, then better agreement of quench time would result. Comparison of results to experimental fluid temperature data shows that CTF overpredicts, which indicates that interfacial heat transfer is possibly being underpredicted. An increase in interfacial heat transfer would better cool the vapor, but this requires more droplet entrainment because it reduces the amount of droplets leaving the top of the bundle.

This study has provided an initial assessment of the CTF LOCA capabilities and led to the correction and improvement of several models in the code. However, other findings indicate that the models require further assessment, including important models that were not yet assessed as part of this study. Including another data set which includes more separate effects testing, such as rod bundle heat transfer (RBHT) [27], would also help to further improve LOCA modeling capabilities. A more in-depth analysis of these results will be provided in forthcoming publications [28,29].

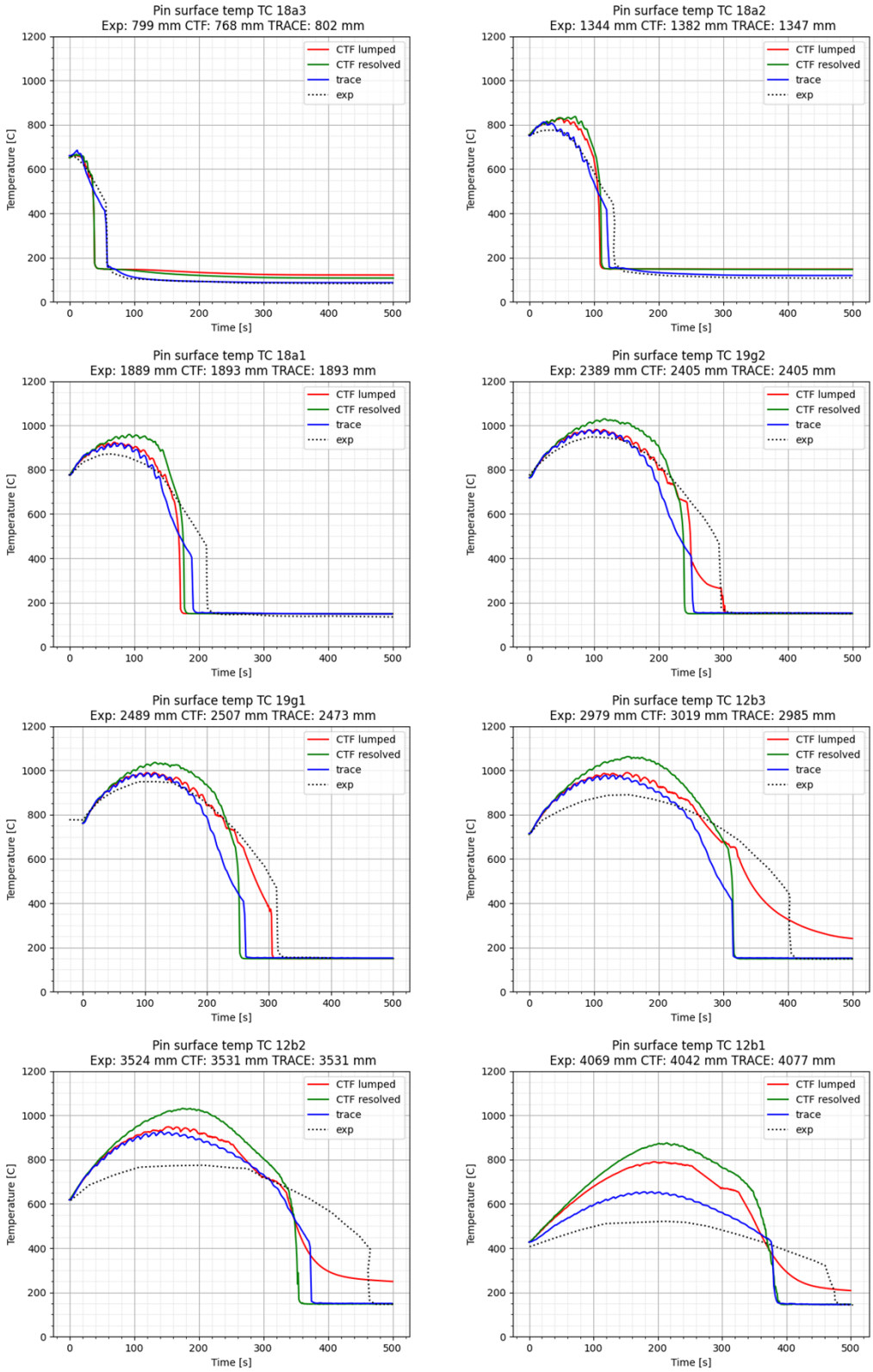

Figure 31. Transient clad surface temperature prediction by TRACE and CTF compared to experimental data for low flooding rate case.